

Flux Phase as a Dynamic Jahn-Teller Phase: Berryonic Matter in the Cuprates?

R.S. Markiewicz and C. Kusko

Physics Department and Barnett Institute, Northeastern U., Boston MA 02115

There is considerable evidence for some form of charge ordering on the hole-doped stripes in the cuprates, mainly associated with the low-temperature tetragonal phase, but with some evidence for either charge density waves or a flux phase, which is a form of dynamic charge-density wave. These three states form a pseudospin triplet, demonstrating a close connection with the $E \otimes e$ dynamic Jahn-Teller effect, suggesting that the cuprates constitute a form of Berryonic matter. This in turn suggests a new model for the dynamic Jahn-Teller effect as a form of flux phase. A simple model of the Cu-O bond stretching phonons allows an estimate of electron-phonon coupling for these modes, explaining why the half breathing mode softens so much more than the full oxygen breathing mode. The anomalous properties of O^{2-} provide a coupling (correlated hopping) which acts to stabilize density wave phases.

I. INTRODUCTION

In a (molecular) Jahn-Teller (JT) effect, an electronic degeneracy in a symmetric molecule is lifted by distorting the molecule and lowering the free energy by an amount E_{JT} . A *dynamic* JT (dJT) effect arises when there is a degeneracy both of electronic levels and of molecular vibrations (strictly speaking, when two independent distortions have the same JT energy lowering). Quantum tunneling between the two distortions restores the (time-averaged) symmetry of the molecule, but leads to a net orbital angular momentum which is half-integrally quantized^{1,2}. In principle, an analog of the dJT effect should exist in dense solids^{3,4}, but this feature of ground state nuclear motion has not been adequately described. Recently, a number of proposals have been made for solid state systems with finite orbital angular momentum in their groundstates, including ‘Berryonic matter’⁵ and the flux phase⁶⁻⁹ or orbital antiferromagnet^{10,11}. Here the connection between these concepts is worked out, a formalism is presented for describing the dJT effect in terms of phonon-assisted flux phases.

This result is particularly timely, since dJT effects have been proposed to play a role in a number of materials of current interest, including buckyballs^{12,5}, cuprates¹³⁻¹⁵, and manganites¹⁶. Remarkably, many of these materials display stripe phases and/or high temperature superconductivity, and it has been proposed that either strong electron-phonon coupling^{17,18} or flux phases may be responsible for these features. Moreover, in the cuprates,

there is recent evidence for both the flux phase¹⁹ and for strong phonon anomalies^{18,20-25}. Hence, the present formalism is applied to a simple model of the in-plane phonons in the cuprates.

The two JT modes plus the dJT state can be combined into a ‘pseudospin’ triplet²⁶ of site charge-density wave (CDW), bond CDW, and flux phase (dynamical CDW). Restricted to a single four-copper plaquette ‘molecule’, they reduce to an $E \otimes (b_1 + b_2)$ JT problem. The site and bond CDW’s can be related to important phonon modes in the cuprates, namely the oxygen breathing mode and a shear mode which couples to the tilting mode associated with the low-temperature tetragonal (LTT) phase. Since there is considerable interest in the flux phase, some care is taken to analyze it in terms of the associated structural distortions. In particular, the anomalous π phase is just the Berry phase of the dJT effect. In the molecular problem, the dJT effect arises at a (weak) degeneracy point; remarkably, at this point the dynamics is (classically) chaotic.

Our model calculations find a crossover from an anti-ferromagnetic insulator at half filling to a doped paramagnetic phase stabilized by density wave order. (The detailed doping dependence is probably complicated by the presence of stripes, as discussed in the Appendix.) The density wave is predominantly stabilized by electron-electron interaction, but with a significant structural component. The system is close to but probably not at the dJT degeneracy point, with the shear and flux phases lying lowest in energy.

This paper is organized as follows. Section II surveys the various phonons which experimentally are found to couple to the holes, and shows that they fall into three classes, including site and bond CDW’s and the flux phase. It is explained how the bond CDW couples to LTT and dimpling distortions. (In an Appendix additional evidence is presented that the coupling is particularly strong in the hole-doped regions, i.e., on charged stripes.) Section III shows that these classes have a well-defined group (pseudospin) structure (Section IIIA), and are closely associated with the dJT effect of a square molecule (IIIB). Section IIIC generalizes the pseudospin formalism to a lattice. In Section IV these results are applied to the cuprates, using both a three band (IVA) and a one band (IVB) model to estimate the electron-phonon coupling of a large number of planar bond stretching modes, including some outside of the above three classes. The reason why the half breathing mode is so strongly renormalized is explained. A simple model of phononic flux phases is presented which can provide a basis for

a general theory of band dJT effects. In Section V the self-consistent gap equations are solved for combined electron-electron and electron-phonon coupling, and it is found that the anomalous behavior of the O^{2-} molecule leads to a particular form of correlated hopping which helps stabilize paramagnetic CDW phases. Some discussion of *desiderata* for a more complete model are presented in Section VI, and conclusions are presented in Section VII.

II. CLASSIFICATION OF PHONON MODES

There is considerable evidence for strong electron-phonon coupling effects in the cuprates. While the effects are weaker than in the nickelates and manganites, we postulate that it is this relative weakness which allows superconductivity to compete against charge ordering. The difficulty in analyzing the coupling lies in the fact that it is spread over so many different modes, and the modes vary from cuprate to cuprate. Here we show that the strongly coupling modes can be classified into three groups: site and bond CDW's and flux phases. Additional evidence specifically tying the phonons to the charged stripes is presented in the Appendix.

The three categories of phonons can be described in different ways. Perhaps the simplest is as site CDW (leading to pileup of charge on alternate Cu's) vs bond CDW's (pileup on oxygens) vs dynamic interchange of the two (the flux or orbital antiferromagnetic – OAF – phase). Alternatively, since the modes all couple strongly to a Van Hove singularity (VHS), the first two may be classified by how they split the VHS peak: the site CDW's leave the X and Y ($(\pi, 0)$ and $(0, \pi)$) point VHS's equivalent, but split each (as in the one-dimensional Peierls transition); the bond CDW's make the X and Y points inequivalent.

A. Breathing Modes

Strong coupling to oxygen breathing modes is found in a number of cuprates. Weber²⁷ originally suggested that there should be large coupling of the electrons to the oxygen breathing mode at (π, π) . However, this mode is suppressed near half filling by strong coupling effects, since the CDW requires a charge imbalance on different copper atoms. The coupling is enhanced by proximity to the VHS, and hence could lead to a CDW instability near optimal doping^{14,17,28,29}. Experimentally, breathing modes appear more strongly coupled near $(\pi, 0)$ than at (π, π) , both in $\text{La}_{2-x}\text{Sr}_x\text{CuO}_4$ (LSCO) and $\text{YBa}_2\text{Cu}_3\text{O}_{7-\delta}$ (YBCO)³⁰. McQueeney, et al.²⁰ have found that the phonon spectra show evidence for a dynamic period doubling in the $\Gamma - (\pi, 0)$ direction, which they associate with stripes. Since this period is independent of doping²¹, it is unlikely to be related to stripe

periodicity, but could be associated with charge ordering *along* the stripes. A possible explanation for the strong coupling of this half breathing mode is given in Section IVA. Very similar anomalies are found in the nickelates, with phonon softening and splitting over a large part of the Brillouin zone, including evidence for local modes tied to stripes³¹. In LSCO, stripe correlations have a strong effect on these oxygen-related phonons near 70 meV^{22,23}.

In this same energy range (50-70meV below the Fermi level), photoemission measurements^{32,33} have found a break in the dispersion of the cuprates, present throughout k -space, although having much more dramatic effects near $(\pi, 0)$. While there are alternative interpretations³³, it has been proposed¹⁸ that this is the conventional renormalization associated with strong electron-phonon coupling³⁴ to the breathing mode phonons near this energy. Such renormalization can produce the extended saddle points observed near $(\pi, 0)$ ³⁵.

B. Relation of Shear Mode to LTT, Dimpling, etc.

Evidence for proximity to a shear mode instability has been noted in LSCO near the 1/8th anomaly, in the form of softening of the $C_{11} - C_{12}$ elastic modulus³⁶. However, it is remarkable that, whereas theoretically there should be a strong electron-phonon coupling with *bond stretching* modes, the observed soft modes are *bond bending* modes, with different modes in each family of cuprates: the low-temperature orthorhombic (LTO) and LTT tilts in LSCO, a dimpling mode in YBCO, and a rotation of the four planar oxygens about the central Cu in the electron-doped cuprates³⁷. Here, we suggest that there is a connection between these modes and the shear instability.

We first consider LSCO. It is a common finding that the local structure in the cuprates differs from the average structural order determined by neutron or x-ray diffraction³⁸, and it has been suggested that the observed LTO phase in LSCO is really dynamically disordered, with the local order being closer to LTT¹⁵. There have been numerous hints of local LTT order³⁹⁻⁴⁴, but the problem is complicated by the simultaneous occurrence of stripe order. The issue of the relation between stripe order and the LTT distortion is addressed in the Appendix. Here, we merely note that the relevant local distortion is likely to be of LTT form, and explore the connection of this distortion to the shear mode.

By increasing the Cu-O bond length along the tilted bonds, both the shear and the LTT distortions make the two oxygens in a unit cell crystallographically inequivalent, thereby coupling to the VHS. Such VHS splitting has recently received renewed interest^{45,46}. We have suggested that the LTT tilt is a secondary modification of a shear mode instability due to lattice mismatch effects³⁵: the underlying instability is to a shear (making inequivalent bondlengths), but the CuO_2 planes are under com-

pression, so the LTT tilt arises as a compromise, making the Cu-O bondlengths inequivalent, without increasing the net Cu-Cu bondlength. Qualitatively, the LTT tilt pattern arises because the CuO_6 octahedra tilt as rigid units⁴⁷: since the octahedra are corner sharing, alternate octahedra must tilt in opposite directions, leading to a distortion at wave vector $\vec{Q} = (\pi, \pi)$. (The detailed interpretation involves partial hole localization on oxygens, and the large size difference between O^- and O^{2-} .³⁵)

Similar effects arise in other cuprates. Thus, high energy phonons behave similarly in LSCO and YBCO, but at low frequencies there are very different structural distortions. In YBCO there is little evidence for an LTT phase (although there was a report of a local tilt-mode instability⁴⁸). More likely, the role of the LTT distortion is taken by the *dimpling mode*. While this mode involves predominantly copper and oxygen motion out of the CuO_2 planes, it also couples to in-plane Cu-O displacements. In particular, it couples to the orthorhombicity⁴⁹, and hence to the same shear mode involved in the LTT phase (distortion B_1 in Fig. 2 below). Hence the dimpling also splits the VHS's, but in a different pattern⁵⁰. Experimentally, the distortion competes with superconductivity, and a large decrease of the orthorhombicity is found both at and below T_c ⁵¹, while a discontinuous change in the dimpling is found on passing through optimal doping⁵². *Chain ordering* also plays a role, since it splits the degeneracy of the VHS's along and across the chain direction. Photoemission seems to find that the VHS along X (Y) is below (above) the Fermi level⁵³, while neutron scattering⁵⁴ finds that the stripes align along the chain direction, reminiscent of LTT pinning. In a related 123 compound, $(\text{La}_{1-x}\text{Ca}_x)\text{-(Ba}_{1.75-x}\text{La}_{0.25+x})\text{Cu}_3\text{O}_y$, the La^{3+} at the Ba site disrupts the chains, leading to an average tetragonal structure; in this case a plane buckling is observed, which is *largest at the doping of optimal superconducting T_c* .⁵⁵

A similar effect is found in $\text{Bi}_2\text{Sr}_2\text{CaCu}_2\text{O}_{8+\delta}$ (Bi2212). The 'ghost' Fermi surfaces in Bi2212 are clear evidence for a lattice period doubling, and a connection with the antiferromagnetic order has been suggested⁵⁶. However, since they are present at room temperature and at optimal doping – far from the region where strong magnetic correlations would be expected – they may instead be related to a structural transition – the known orthorhombic ordering⁵⁷. This lattice anomaly also couples strongly to the VHS. Most suggestively, it has recently been found that *the intensity of these ghost features peaks near optimal doping*⁵⁸. This is close to the prediction of the VHS stripe model, in which the structural order should be maximal in the slightly overdoped regime, just when magnetic correlations disappear (termination of the stripe phase).

C. The Flux Phase

The flux phase has generated intense interest because of its highly unusual physical properties. The experimental evidence for this phase, which remains controversial, includes (i) the fit of the dispersion of the Mott insulator $\text{Sr}_2\text{CuO}_2\text{Cl}_2$ (SCOC)⁵⁹ to the flux phase form⁷ (however, alternative interpretations include a Mott antiferromagnet, while more recent experiments find a more complex dispersion⁶⁰), (ii) the d-wave-like nature of the normal-state pseudogap⁶¹, which has been interpreted in terms of the conical point (node) in the flux phase dispersion at $(\pi/2, \pi/2)$, and (iii) the recent observation of the induced magnetic fields associated with the orbital currents¹⁹. (However, more recent measurements⁶² find that the magnetic moment lies in-plane, and not along the c-axis as originally expected, and the experiment also has alternate interpretations⁶³.)

D. Competition and Cooperation of the CDW's

In Section IIIB, we will show that the molecular equivalent of the flux phase, the dJT state, arises from competition between the two other modes. In the cuprates, there is also evidence for a competition between the two types of CDW, which we briefly review here. In LSCO, both the breathing and the LTT modes show anomalous softening with doping. An interesting situation arises in YBCO. Pintschovius and Reichardt (p. 349 of Ref. 30) note that hole doping may renormalize the half-breathing mode phonon frequency from 74meV to ~ 37 meV, due to a special form of Van Hove nesting⁵⁰. The mechanism proposed involves VHS induced coupling of two phonon modes remarkably similar to the flux phase effects we are describing. The dimpling of the CuO_2 planes causes the VHS's to bifurcate (e.g., the X VHS splits along the $\Gamma - X - \Gamma$ line). In turn, nesting between the bifurcated peaks leads to breathing mode softening along $\Gamma - X$ and can lead to a period doubling instability. The exact nesting wave vector is controlled by the degree of VHS bifurcation, which in turn depends on the amount of dimpling. Thus, two phonon modes (here the dimpling and half-breathing modes) are strongly coupled by the VHS. A similar competition between breathing and octahedral tilt modes near a superconducting instability is found⁶⁴ in $\text{Ba}_{1-x}\text{K}_x\text{BiO}_3$; in this case the tilt modes are near the R point of the Brillouin zone, coupling to the three-dimensional VHS's.

Other routes to mode coupling are also possible. For example, when the breathing mode softens^{30,20,21}, it can couple to a lower frequency phonon, either an LTT distortion in LSCO or a dimpling mode in YBCO, and drive that second mode soft. This strong mixing of the two modes can create a flux phase.

III. ELECTRON-PHONON COUPLING: FROM SQUARE MOLECULES TO CUPRATES

In this section, we show that the three phonon modes form a symmetry group, and map the interaction to a molecular JT model. We demonstrate that the same degeneracy arises in both the molecular and lattice problems. In Section IV we apply these results to the cuprates, showing how the phonons in LSCO fit into the scheme, and calculating their coupling to electrons.

A. The Pseudospin Group

We begin with a purely theoretical description, based on the group theory of instability, or spectrum generating algebras⁶⁵, specialized to the VHS instability group^{11,66}, of SO(8) symmetry. Within this group there is a triplet of CDW operators, which couple strongly to phonons. These operators are spanned by an $SU(2)$ subalgebra which we call ‘pseudospin’.

To specify the order parameters in terms of bilinear electronic operators, it is necessary to define these operators on a *larger unit cell*, containing a plaquette of four copper atoms. It is convenient to introduce creation operators $a_{\pm,\sigma}^{\dagger}(\vec{r}) = (\psi_{E_{u1},\sigma}^{\dagger}(\vec{r}) \pm \psi_{E_{u2},\sigma}^{\dagger}(\vec{r}))/2$. The pseudospin can be written in terms of the Fourier transforms of these states. In the basis

$$\{B_{\sigma}(k)\} = \{a_{+,\sigma}(\vec{k}), a_{-,\sigma}(\vec{k})\}, \quad (1)$$

the explicit form of these matrices is

$$\tilde{\tau} = \frac{\tilde{\gamma}}{2}\tilde{T}_x, \quad (2)$$

$$\tilde{O}_{OAF} = \frac{\tilde{\gamma}}{2}\tilde{T}_y, \quad (3)$$

$$\tilde{O}_{CDW} = \tilde{T}_z, \quad (4)$$

where

$$\tilde{T}_x = \begin{pmatrix} 0 & 1 \\ 1 & 0 \end{pmatrix}, \quad (5)$$

$$\tilde{T}_y = \begin{pmatrix} 0 & -i \\ i & 0 \end{pmatrix}, \quad (6)$$

$$\tilde{T}_z = \begin{pmatrix} 1 & 0 \\ 0 & -1 \end{pmatrix}, \quad (7)$$

with $c_i = \cos k_i a$ and $\tilde{\gamma} = c_x - c_y$. The operators \tilde{O}_{CDW} , $\tilde{\tau}$, and \tilde{O}_{OAF} transform exactly as a pseudospin near the VHS’s ($c_x - c_y = \pm 2$), but not at a general point in the

Brillouin zone. This same problem arises in SO(5)⁶⁷, and the Henley operator⁶⁸ was introduced to deal with it.

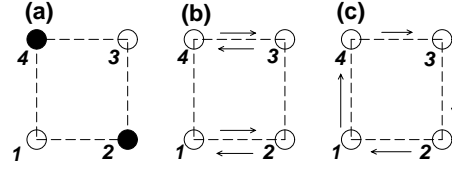


FIG. 1. Pseudospin triplet: O_{CDW} (a), τ (b), O_{OAF} (c).

The electronic arrangements corresponding to these operators are illustrated in Fig. 1: O_{CDW} is a site CDW, with excess charge on the odd sites 1 and 3, and a deficit on the even sites 2 and 4; τ is a bond centered CDW, with excess charge on the 1-2 and 3-4 links, and a deficit on the 1-4 and 2-3 bonds; while O_{OAF} is an orbital antiferromagnet, with an orbital current flowing clockwise, from $1 \rightarrow 4 \rightarrow 3 \rightarrow 2$. In a three-band model, O_{CDW} would represent a Cu-based CDW, and τ an O-based CDW. Note that the CDW mode is equivalent to the charge ordering found in $\text{La}_{2-x}\text{Sr}_x\text{NiO}_4$ for $x \sim 0.5$ ⁶⁹. The orbital current operator¹¹ O_{OAF} is closely related to the flux phase⁶. In the flux phase, hopping is accompanied by an accumulation of a phase change by π on circulating a plaquette. For the plaquette of Fig. 1c, this leads to a contribution to the Hamiltonian proportional to

$$H' = e^{i\pi/4}(a_2^{\dagger}a_1 + a_3^{\dagger}a_2 + a_4^{\dagger}a_3 + a_1^{\dagger}a_4) + h.c. \\ = \frac{1}{\sqrt{2}}(a_2^{\dagger}a_1 + a_3^{\dagger}a_2 + a_4^{\dagger}a_3 + a_1^{\dagger}a_4 + h.c.) - 2\sqrt{2}T_y. \quad (8)$$

The first term in Eq. 8 corresponds to an (uninteresting) uniform hopping on the plaquette. Thus, up to this term, *the flux phase is equivalent to the orbital antiferromagnet O_{OAF} (T_y).*

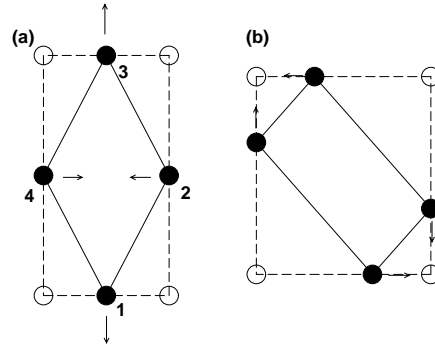


FIG. 2. B_1 (a) and B_2 (b) distortions of Cu_4O_4 . Open (filled) circles represent the Cu’s (O’s).

While the instabilities are predominantly electronic, they are accompanied by lattice instabilities, as in the Peierls transition. In particular, the CDW couples to

the oxygen breathing mode and the τ -mode couples naturally to a shear distortion; these are referenced to a single molecule in Fig. 2. The relation of this shear to the LTT tilting mode was clarified in Section II.

This pseudospin triplet is an exact condensed-matter analog to the molecular JT modes responsible for the dJT effects found in molecules. The enlarged unit cell associated with Eq. 1 provides a natural connection. Thus, we regard the CuO_2 planes as composed of a square array of Cu_4O_4 ‘molecules’ bonded to each neighbor by a pair of oxygens. These molecules can be embedded into the lattice in two equivalent ways, as illustrated in Fig. 3. While it is simpler to analyze a square lattice of square molecules, as in Fig. 3a, a more accurate representation is in terms of a ‘centered square’ lattice as in Fig. 3b. [Crystallographically, the centered square is not a primitive unit cell, but it is convenient for the present purposes.] The latter case has twice as many molecules, but they are corner sharing. The atoms (coppers and oxygens) in each molecule deform in the same way. For instance, Fig. 3c illustrates the flux phase, labelling each square plaquette which contains a $+\pi$ flux with a plus sign. When interpreted as in Fig. 3b, the ground states have a two-fold degeneracy, which is also found in the flux and CDW phases.

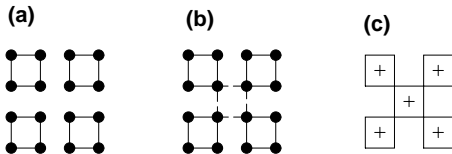


FIG. 3. Berryonic matter: two views of the lattice of square molecules, either as simple square (a) or as centered square with corner sharing molecules (b) compared with the flux phase (c), where the +’s indicate plaquettes with a $+\pi$ flux.

The above analysis resolves an old conundrum. Earlier calculations interpreted the LTT phase in terms of a Van Hove – Jahn-Teller (VHJT) effect^{15,29}, where the electronic degeneracy is associated with the presence of two VHS’s. This is puzzling, since JT effects usually have a simple molecular basis, but such a basis is not obvious in the present case. We now see that the VHJT effect on the conventional lattice is equivalent to a conventional JT effect on a supercell lattice. The resulting lattice constitutes a nearly exact realization of a Berryonic crystal – replacing the originally proposed⁵ JT active triatomic molecules by square molecules.

The close connection between the JT and Van Hove viewpoints can be clarified by representing the CuO_2 plane electronic states in a supercell representation^{15,66}, replacing the copper (or Zhang-Rice singlet) wavefunctions by electronic states symmetrized on a single plaquette. These states $\psi_{+ijk} = (\psi_1 + i\psi_2 + j\psi_3 + k\psi_4)/2$ have A_{1g} (ψ_{++++}), B_{2g} (ψ_{+--+}), and E_u (ψ_{++--} , ψ_{--++}) symmetry. Including nearest (t) and next-nearest neighbor

(t') hopping, the kinetic energies are

$$\begin{aligned} E(A_{1g}) &= -2t - t', \\ E(E_u) &= t', \\ E(B_{2g}) &= 2t - t', \end{aligned} \quad (9)$$

so at half filling, the A_{1g} level is filled and there are two electrons in the E_u levels. Optimal doping corresponds to one extra hole per plaquette, leaving one electron in the E_u levels, and a JT effect. The full band dispersion of the square lattice can be written as a superposition of these four states (Appendix I of Ref. 15). It is found that *all states near the VHS’s are built up exclusively of E_u states*. On the other hand, states near the nodal points have A_{1g} character. Note that this explicitly demonstrates that VHS instabilities persist down to ‘lattices’ as small as a single 2×2 plaquette.

The above calculations are for the weak coupling limit, and are consistent with the charge ordered states found in Section V. However, the analysis can be repeated in the strong coupling limit. Thus, for an antiferromagnetic arrangement, the (mean field) energies are $E(A_{1g}) = E(B_{2g}) = -t' - \sqrt{U^2 + 4t'^2}$, $E(E_u) = t' - \bar{U}$, with $\bar{U} \simeq U/2$. With parameters¹¹² $t \simeq 325\text{meV}$, $U/t \simeq 6$, $t'/t \simeq -0.276$, and $J = 4t^2/U$, $E(E_u) - E(A_{1g}) \simeq 2t' + J \simeq t/6 > 0$, so the first hole would again come from the E_u level, although all levels are close in energy. (Note that a smaller J would reverse the order of the levels but would still lead to an electronic degeneracy.) Thus, one can still have a JT instability in the strong coupling limit, although its nature can be significantly modified. For a somewhat different example, see Ref. 70.

The present JT effect is significantly different from the conventional JT effect of a CuO_6 octahedron, which involves the electronic (pseudo-)degeneracy associated with the Cu d_{z^2} and $d_{x^2-y^2}$ orbitals. Many earlier studies (e.g., Refs. 13, 71) have proposed that this (pseudo)JT effect plays an important role in cuprate physics. The present model works even if the d_{z^2} orbitals are completely uncoupled (although a residual coupling could enhance the present effects). The model is closer to the large polaron limit^{72,73}, but with a particular choice of polaronic coupling dictated by the underlying $\text{SO}(8)$ symmetry.

B. The Molecular Jahn-Teller Effect

As a preliminary to studying the VHJT effect on a lattice, we first look at the molecular analog, a Cu_4O_4 molecule with square planar symmetry, D_{4h} , which corresponds to the $E \otimes (b_1 + b_2)$ JT problem^{4,74,75}. This molecule can display a dJT effect which bears a striking resemblance to the flux phase. Figure 2 displays the relevant B_1 and B_2 distortions, assuming predominantly oxygen vibrations. The B_2 distortion is the oxygen breathing mode, while the B_1 has the form of the shear wave associated with the LTT instability.

The JT energy can be written $E_{JT}^{(i)} = V_i^2/(2M\omega_i^2)$, where V_i is the electron-phonon coupling and M is the ionic mass. In terms of E_{JT} , there are three classes of solution:

- (i) $E_{JT}^{(1)} \neq E_{JT}^{(2)}$,
- (ii) $E_{JT}^{(1)} = E_{JT}^{(2)}$ but $\omega_1 \neq \omega_2$,
- (iii) $E_{JT}^{(1)} = E_{JT}^{(2)}$ and $\omega_1 = \omega_2$.

For case (i) the lowest energy state consists of a static JT distortion of the mode with larger JT energy only. This simple case may apply to the cuprates: it has long been a puzzle why the oxygen breathing modes do not display the large softening expected²⁷ near (π, π) . On the other hand, the LTT mode is quite soft, and nearly unstable. This would follow if $E_{JT}^{(1)} > E_{JT}^{(2)}$. The results of Section V are consistent with this possibility. However, formally the special cases (ii) and (iii) are more interesting, allowing dynamic solutions which are closely related to the flux phase.

Case (iii) reduces exactly to the well-known $E \otimes e$ problem of the triatomic molecule^{1,2,76}, and *the electronic wave function is double valued*: when the molecular motion undergoes a 2π rotation, the electronic wave function picks up an extra factor of π , the Berry phase^{76,77}. However, in the cuprates the phonon frequencies are very different (Section IV), so case (iii) does not apply. Nevertheless, condition (ii) (weak degeneracy) may hold approximately in the cuprates, and it is known that inclusion of quadratic vibronic coupling enhances the range of case-(ii) degeneracy⁷⁸. This special case has recently been analyzed⁷⁵: the dJT effect with π Berry phase is preserved, although the classical motion may be *chaotic*.

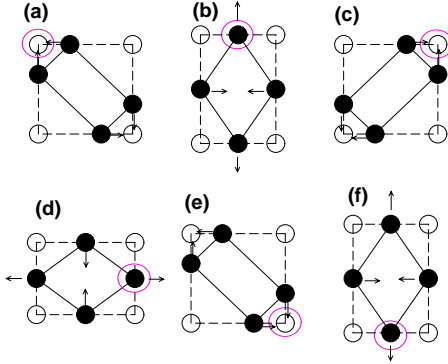


FIG. 4. Dynamic JT rotation mixing B_1 and B_2 modes of O_4 . Large open circle represents one hole. Each time step (a-f) represents one quarter of a cycle of molecular rotation, so in frame e the molecules have completed one cycle of rotation with respect to frame a, while the hole has completed only half a rotation.

The origin of the wave function sign change is explained in Fig. 4. As each oxygen atom rotates about its undistorted position, the hole (large circle; a second hole is in the symmetric position) rotates about a different origin, the center of the square. When the individual atoms

complete one full rotation, the hole has only completed half of a rotation, just as in the triangular molecule¹. In analogy with the triatomic molecule, the electronic wave function can be kept single valued by multiplying it by a phase factor, $e^{i\theta/2}$.

Thus, the dJT effect with anomalous Berry phase exists for a square molecule; while some ‘fine tuning’ of the parameters is required, this may arise from quadratic vibronic coupling⁷⁸. In the following subsection, we will see that a similar accidental degeneracy exists for the lattice problem, and it is known that the structural transitions in LSCO are strongly nonlinear^{14,79}. However, in Section VC it will be seen that on a lattice the flux phase can be stabilized over a wider parameter range, even without nonlinear coupling.

C. Extension to the Lattice

The $E \otimes (b_1 + b_2)$ problem has been extended to the lattice⁸⁰ but only the nondegenerate case (i) has been analyzed in detail. Here, we demonstrate that the degenerate case (ii) remains a possibility. On a lattice, the JT coupling becomes

$$H_{JT} = \sum_{i=1,2} H_{JT,i} \quad (10)$$

$$H_{JT,i} = -\eta_i e_i \sum_{\vec{l}} \tau_i(\vec{l}) - \sum_{\vec{q}} \sum_m v_i^m(\vec{q}) Q_i^m(\vec{q}) \tau_i(-\vec{q}), \quad (11)$$

where the m -sum is over different phonon branches of a given symmetry, and we include coupling to the elastic strains, with e_i and η_i the strain component and its coupling to τ_i . If the phonon Hamiltonian is written

$$H_{ph} = \frac{1}{2} \sum_{i,m,\vec{q}} M\omega_{i,m}^2 Q_i^m(\vec{q}) Q_i^m(-\vec{q}), \quad (12)$$

with M an appropriate ionic mass, then the linear coupling to Q_i can be replaced by an effective electron-electron coupling by the displaced oscillator transformation:

$$\hat{Q}_i^m(\vec{q}) = Q_i^m(\vec{q}) + \frac{v_i^m(-\vec{q}) \tau_i(\vec{q})}{M\omega_{i,m}^2}, \quad (13)$$

This transformation approximately decouples the phonons, leaving an interaction

$$H_{int} = - \sum_{i,\vec{l}} \eta_i e_i \tau_i(\vec{l}) - \frac{1}{2} \sum_{i,\vec{q}} J_i(\vec{q}) \tau_i(\vec{q}) \tau_i(-\vec{q}), \quad (14)$$

with $J_i(\vec{q}) = \sum_m K_i^m(\vec{q})$,

$$K_i^m(\vec{q}) = \frac{v_i^m(\vec{q}) v_i^m(-\vec{q})}{M\omega_{im}^2(-\vec{q})}. \quad (15)$$

This decoupling is only approximate, since the \hat{Q} 's depend on the τ 's, so that they do not obey canonical commutation relations. It will, however, be adequate for the present purposes. At mean field level,

$$\eta_i \langle e_i \rangle = \mu_i \langle \tau_i \rangle, \quad (16)$$

with $\mu_i = N\eta_i^2/2c_i^0$ and c_i^0 the bare elastic constant. Letting⁸⁰

$$\lambda_i = \mu_i + \sum_m (K_i^m(0) - \frac{1}{N} \sum_{\vec{q}} K_i^m(\vec{q})), \quad (17)$$

and assuming only one Δ_i is non-vanishing, the gap equations are

$$\Delta_i = \lambda_i \langle \tau_i \rangle, \quad (18)$$

$$\langle \tau_i \rangle = - \sum_{\vec{k}} \Delta_i \frac{f(E_+(\vec{k})) - f(E_-(\vec{k}))}{E_+(\vec{k}) - E_-(\vec{k})}, \quad (19)$$

with E_{\pm} the energy eigenvalues and $f(E)$ the Fermi function. If $\lambda_1 \neq \lambda_2$, only the mode with larger λ_i has nonzero expectation value, although both modes can soften above the transition temperature. However, when

$$\lambda_1 = \lambda_2 \quad (20)$$

then $\Delta_1 = \Delta \cos \theta_0$, $\Delta_2 = \Delta \sin \theta_0$, with θ_0 arbitrary. Equation 20 is the generalized version of condition (ii).

IV. APPLICATION TO THE CUPRATES

A. Bond Stretching Modes in LSCO Three-Band Model

In Section V, we will calculate the mean-field properties of the various CDW's, combining electron-electron and electron-phonon interaction and including strong coupling corrections and competition with the Mott gap. Here we develop a simple model for estimating the electron-phonon interaction. We introduce a three-band model, and apply it to a number of phonon modes which have been proposed to play a role in the cuprates. In the following subsection, we will reduce the model to a one-band version.

We concentrate predominantly on CuO_2 plane phonons associated with in-plane vibrations, and particularly on Cu-O bond stretching phonons. Mott's original picture of a metal-insulator transition involved a loss of covalency as a lattice is gradually expanded. Hence, near a Mott transition it would be expected that bond-length changing phonons might play an important role, modulating a crossover from covalent to ionic behavior⁸¹. Figure 5 shows the phonon dispersion in La_2CuO_4 along the $(\zeta, \zeta, 0)$ (Σ) direction, calculated by Wang, et al.⁸².

Shown in bold are the branches which are predominantly associated with in-plane Cu-O vibrations. (Wang, et al. provide the wave functions only along the high symmetry axes, Γ and X ; the remainder of the curves are an interpolation based on symmetry. Note the anti-crossing behavior evident on several branches.) The pattern of distortion for a number of modes of interest is also shown, including the breathing²⁷, half-breathing^{20,81} (at $(\pi, 0)$), dimer⁸³, quadrupole¹³, ferroelectric⁸¹, and shear³⁵ modes. This by no means exhausts all relevant modes. Among modes which are not modeled are the LTT tilt mode and various c -axis modes⁸⁴. As discussed above, we treat the LTT mode as a secondary modification of the shear mode instability.

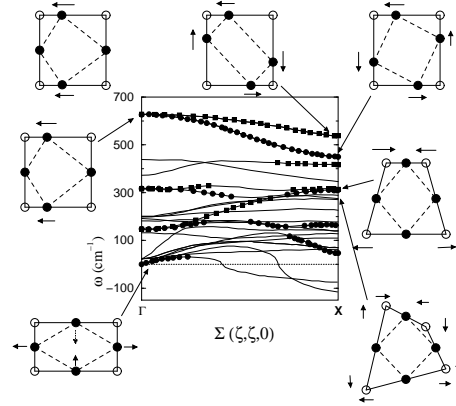


FIG. 5. Phonon modes of the CuO_2 planes, including distortion patterns for several Cu-O bond stretching modes. Clockwise from top left: half-breathing, breathing, quadrupole, dimer I, dimer II, shear, and ferroelectric modes. Filled squares (circles) = Σ_1 (Σ_3) branches predominantly representing the CuO_2 planes.

In order to estimate how strongly these modes couple to the electrons, we analyze a simple three-band dispersion for the CuO_2 plane, with parameters t_0 (t'_1) for Cu-O (O-O) hopping, and Δ_0 (Δ_1) for Cu (O) site energy. The electron-phonon coupling is assumed to arise via modulating these parameters. Thus, a change δu in the Cu-O bondlength a produces a change

$$\delta t = -\beta t_0 \delta u / a \quad (21)$$

in t_0 and a change

$$\delta_0 = \alpha_d \Delta_0 \delta u / a \quad (22)$$

in Δ_0 (or Δ_1). We estimate $\beta \sim 3.5\alpha_t$ ^{29,85} ($\alpha_t = 1$) and α_d from a Madelung contribution as $\alpha_d = qe^2/\epsilon_0 a \Delta_0 \sim 0.55$, for $\Delta_0 \sim 4eV$, effective charge $q = 2$ (O^{2-} or Cu^{2+}) and dielectric constant $\epsilon_0 \sim 5$. In the following, we will treat the α 's as dimensionless parameters of order unity in order to scale the electron-phonon coupling. The net change in Δ on any site is then $(n - m)\delta_0$ where n (m) is the number of near neighbors that move closer to (further away from) the given site. For a frozen lattice

distortion of amplitude $\pm\delta u$, we calculate how the net electronic energy changes. Model parameters include the position of the Fermi level, the value of t'_1 , and the ratio β/α_d . This last parameter can be thought of as a measure of covalency: increasing Δ tends to localize holes on Cu, making the material more ionic, while increasing t_0 delocalizes holes, increasing covalency. We restrict ourselves here to the following parameters: $t_0 = 1.3eV$, $\Delta_0 = 4eV$, $a = 1.9\text{\AA}$, Fermi level at VHS (in the absence of phonon distortion) at a doping $x = 0.25$ (to achieve this, a large value of $t'_1/t_0 = -1.8$ is assumed); and $\alpha_d = \alpha_t = 1$. The model neglects possible coupling to the Cu d_{z^2} orbital (important for the conventional JT distortions of the quadrupole and breathing modes¹³) and anomalies associated with the near instability of O^{2-} (Section V.C).⁸⁶ The two forms of electron-phonon coupling are similar to those assumed by Yonemitsu, et al.⁸⁷; while the numerical estimates are not identical, we find similar estimates for the coupling to the breathing mode. Their electron-phonon coupling parameters are, in our notation $\lambda_\alpha = \beta^2 t_0 / A_{br} \simeq 0.264$, $\lambda_\beta = \alpha_d^2 \Delta_0^4 / t_0 A_{br} \simeq 0.204 \alpha_d^2 = 0.051$, for $\alpha_d = 0.5$, and $A_{br} = 60.4eV$ from Table III. Yonemitsu, et al.⁸⁷ estimate $\lambda_\alpha = 0.28$ and had no estimate for λ_β .

For the shear modes and the modes at $S = (\pi, \pi)$, the resulting electronic hamiltonian can be written in the form $H =$

$$\begin{pmatrix} \Delta + \delta_1 & -t_1 e_x & -t_2 e_y & 0 & t_3 e_x^* & t_4 e_y^* \\ -t_1^* e_x^* & \delta_2 & -2t'_1 c'_- & t_5 e_x & 0 & -2t'_1 c'_+ \\ -t_2^* e_y^* & -2t'_1 c'_- & \delta_3 & t_6 e_y & -2t'_1 c'_+ & 0 \\ 0 & t_5^* e_x^* & t_6^* e_y^* & \Delta - \delta_1 & -t_7 e_x & -t_8 e_y \\ t_3^* e_x & 0 & -2t'_1 c'_+ & -t_7^* e_x^* & -\delta_4 & -2t'_1 c'_- \\ t_4^* e_y & -2t'_1 c'_+ & 0 & -t_8^* e_y^* & -2t'_1 c'_- & -\delta_5 \end{pmatrix} \quad (23)$$

while for the half breathing mode at $X = (\pi, 0)$, and the ferroelectric mode, $H =$

$$\begin{pmatrix} \Delta + \delta_1 & -t_1 e_x & -2it_0 s'_y & 0 & t_3 e_x^* & 0 \\ -t_1 e_x^* & 0 & -2it'_1 s'_y e_x & t_5 e_x & 0 & 2it'_1 s'_y e_x^* \\ 2it_0 s'_y & 2it'_1 s'_y e_x^* & \delta_3 & 0 & 2it'_1 s'_y e_x & 0 \\ 0 & t_5^* e_x^* & 0 & \Delta - \delta_1 & -t_7 e_x & -2it_0 s'_y \\ t_3 e_x & 0 & -2it'_1 s'_y e_x^* & -t_7 e_x^* & 0 & -2it'_1 s'_y e_x \\ 0 & -2it'_1 s'_y e_x & 0 & 2it_0 s'_y & 2it'_1 s'_y e_x^* & -\delta_3 \end{pmatrix}. \quad (24)$$

Here $e_i = \exp(ik_i a/2)$, $i = x, y$, $c'_\pm = \cos(k_x \pm k_y) a/2$ and $s'_y = \sin k_y a/2$. For the modes at S (the shear mode), $\delta_{i+2} = \delta_i (-\delta_i)$ $i = 2, 3$. Writing $\delta_i = n_i \delta_0$ and $t_i = t_0 + m_i \delta t_0$, then for oxygen vibrations (the breathing, half-breathing, ferroelectric, and quadrupole modes) $m_{i+4} = +m_i$, while for modes involving copper motions (the shear and dimers), $m_{i+4} = -m_i$, $i = 1, 4$. For completeness, we include an extra parameter δ_3 in Eq. 24 which is allowed by symmetry, due to second-neighbor relative motion; however, to make a uniform comparison

with other modes, the value of δ_3 will be set to zero. The remaining elements are listed in Table I.

Table I: Phonon Coupling Parameters

Mode	n_1	n_2	n_3	m_1	m_2	m_3	m_4
1. Breathing	4	0	0	1	1	1	1
2. Half-Breathing	2	0	2	1	-	1	-
3. Quadrupolar	0	0	0	1	-1	1	-1
4. Dimer I	0	-2	0	1	0	-1	0
5. Dimer II	0	-2	2	1	-1	-1	1
6. Dimer III	0	-2	2	1	1	-1	-1
7. Shear	0	-2	2	1	-1	1	-1
8. Ferroelectric	0	0	0	1	-	-1	-

Table II: Energy Parameters

Mode	γ	X_1	X_2
1. Breathing	0	$2X_{10}$	X_-
2. Half-Breathing	0	X_{10}	$2(t_0^2 - \delta t_0^2)c_x$
3. Quadrupolar	0	0	X_-
4. Dimer I	1	0	$X_+ + 4it_0 \delta t_0 s_x$
5. Dimer II	0	0	$X_+ + 4it_0 \delta t_0 (s_x - s_y)$
6. Dimer III	0	0	$X_+ + 4it_0 \delta t_0 (s_x + s_y)$
7. Shear	0	0	$2(t_+^2 c_x + t_-^2 c_y)$
8. Ferroelectric	0	0	$2(t_0^2 - \delta t_0^2)c_x$
9. Flux Dimer I	1	0	$X_- + 4it_0 \delta t_0 c_x$
10. Flux Dimer II	0	0	$X_- + 4it_0 \delta t_0 (c_x - c_y)$
11. Flux Dimer III	0	0	$X_- + 4it_0 \delta t_0 (c_x + c_y)$
12. Flux Shear	0	0	$X_- - 4t_0 \delta t_0 (s_x - s_y)$

The above calculations refer to static (frozen) phonon modes, and hence do not give direct information on dJT modes. In a Hartree-Fock calculation, dynamic modes can be modelled by imaginary order parameters, and in Section V, it is shown that the mean-field decomposition of nearest-neighbor Coulomb repulsion produces a direct coupling to the OAF (flux phase) mode. In this spirit a similar mean-field phonon flux phase can be constructed

from the above by (a) replacing δt_0 by $i\delta t_0$ and (b) making a similar replacement for the δ_i , which involves moving the term to the off-diagonal ($H_{i,i+3}$) position.

The lattice distortions are found by minimizing the sum of the hamiltonian Eq. 24 and a phonon term, Eq. 12, which may be rewritten as $H_{ph} = A(\delta u/a)^2$, where $A = \eta M \omega^2 a^2 / 2$, and A and ω are listed in Table III. Strictly speaking, the phonon frequencies should be bare values, neglecting electron-phonon coupling, but for present purposes we use calculated⁸² or experimental³⁰ values for the undoped insulator La_2CuO_4 . [For the shear mode, $A = (C_{11} - C_{12})a^2 c$, where $(C_{11} - C_{12})/2 = 99\text{GPa}$

[36] and c is the c -axis lattice constant.] The parameter η is one if the distortion is along the X or Y axis only, two if it is along both, and M is the mass of the moving ion, oxygen or copper (or the appropriate average for the ferroelectric mode). These equations must in general be solved numerically, but some insight can be gotten for the special case $n_2 = n_3 = t'_1 = 0$, for which the four non-zero eigenvalues are given by

$$E_{i\pm} = \frac{\Delta_0 \pm \sqrt{\Delta_0^2 + 4W_i^2}}{2}, \quad (25)$$

with $i = \pm 1$, $W_{\pm}^2 = W_1^2 \pm \sqrt{X_1^2 + |X_2|^2}$, $W_1^2 = 4(t_0^2 + (1 - \gamma/2)\delta t_0^2)$ (except for the half breathing and FE modes, for which $W_1^2 = 2(t_0^2[1 + 2s_y'^2] + \delta t_0^2)$) and the X 's and γ 's are listed in Table II, with $s_i = \sin(k_i a)$ (and recall $c_i = \cos(k_i a)$) $X_{\pm} = 2(t_0^2 \pm \delta t_0^2)(c_x + c_y) \mp 2\gamma\delta t_0^2 c_y$ and $X_{10} = 2E\delta_1 + 4t_0\delta t_0$ (note that the solution is only implicit if $\delta_1 \neq 0$). The generic form of X_2 is $X_2 = t_1 t_5 e_x^2 + t_3^* t_7^* e_x^{*2} + t_2 t_6 e_y^2 + t_4^* t_8^* e_y^{*2}$. Note that E_{i+} is the antibonding band which is approximately half filled.

Figure 6 shows the calculated electronic energy shifts up to large distortions $\delta u/a = 0.1$ (local distortions of up to about 5% are reported in EXAFS measurements²⁵). A number of interesting features can be noted. (1) All the distortions lead to highly nonlinear shifts of the electronic energy. (2) While the breathing mode has the strongest coupling (as originally predicted by Weber²⁷), the half-breathing mode also has a large coupling, since δ_1 produces a large splitting at the VHS, Fig. 8. (3) The energy shifts correspond to significant phonon softening, but when the quadratic phonon energy is included, it is found that only the breathing and (marginally) half breathing mode become unstable – the additional softening due to electron-electron coupling is discussed in Section V. Instabilities of the dimer modes were found earlier⁸³, but only in strong nesting conditions – half filling with $t'_1 = 0$. (4) A problem for a pure phonon-flux phase should be noted: the symmetric dimer III mode has a larger energy lowering than the asymmetric ($c_x - c_y$) dimer II mode.

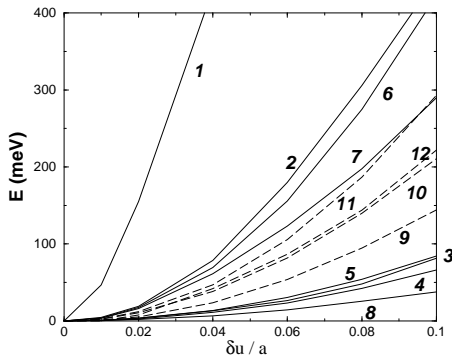


FIG. 6. Energy of various phonon modes of CuO_2 planes, assuming $\alpha_d = 1$ and $\beta = 3.5$, for static (solid lines) or flux phases (dashed lines). The phonon modes are numbered according to Table II.

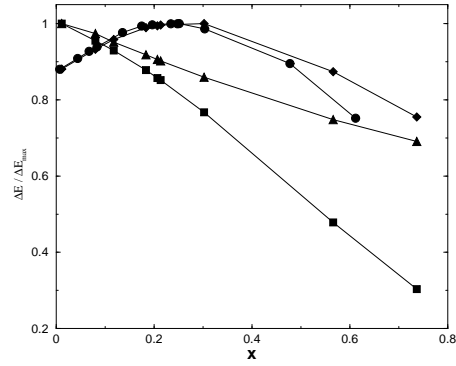


FIG. 7. Doping dependence of the frozen phonon energy lowerings, associated with the breathing mode (circles), half-breathing ($(\pi/a, 0)$ mode (squares), shear mode (diamonds), and dimer III mode (triangles), all normalized to their maximum amplitude. The half-breathing and shear modes have strongest coupling near the VHS. $\delta u/a = 0.04$ for the breathing mode, 0.08 for the others.

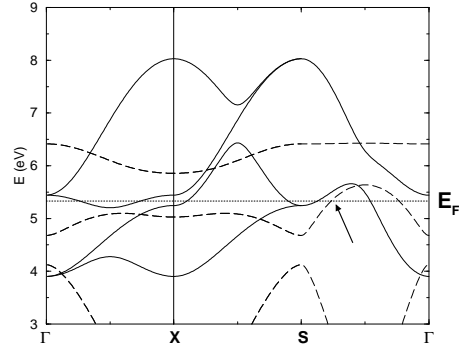


FIG. 8. Three-band dispersion of the CuO_2 planes, in the presence of a frozen breathing mode (dashed lines) or half-breathing ($(\pi/a, 0)$ mode (solid lines) modulation, assuming $\beta/\alpha_d = 3.5$, and $\delta u/a = 0.02$ (breathing) or 0.04 (half breathing). The arrow indicates the breathing mode hole pocket near $(\pi/2a, \pi/2a)$. Brillouin zone special points are $\Gamma = (0, 0)$, $X = (\pi/a, 0)$, $S = (\pi/a, \pi/a)$.

The doping dependence of the energy lowering is shown in Figure 7. The results are in good agreement with experiments²⁰ on both LSCO and YBCO and with LDA calculations⁸⁸ which find that the half-breathing mode softens more than the (π, π) breathing mode. This result is surprising since the breathing mode has stronger coupling. However, this mode has an unusual frustration effect: it opens a complete gap at the Fermi level, Fig. 8, so the Fermi level can only fall in the gap if the band is filled, $x = 0$. To accommodate additional holes, the Fermi level must shift *below* the gap, reducing the electronic energy lowering. Hence optimal doping for this mode is at half filling, and *while there is a large electronic softening of the breathing mode at the VHS, there is an even larger softening near half filling, so a doping dependence would show a hardening of the mode.* Indeed, such a hardening

is observed in the nickelates³¹. This result persists in the presence of strong correlation effects, Section V. For the half-breathing mode correlation effects should enhance the already large softening of the mode with doping, in good agreement with experiment.

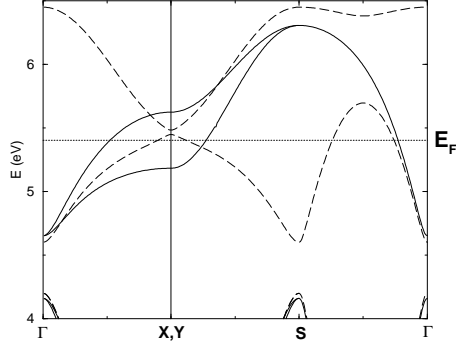


FIG. 9. Three-band dispersion of the CuO₂ planes, in the presence of a frozen dimer II mode (long-dashed lines) or shear mode (solid lines) modulation, assuming $\beta/\alpha_d = 3.5$, and $\delta u/a = 0.04$.

Figures 8-10 compare the dispersions of several of the modes, near the upper (Cu-like) band of the three-band model. For all cases, the magnitude of electronic energy lowering can be directly correlated with the size of the gap at the VHS (X -point). Note that the gap is largest for the breathing mode, but the Fermi level lies below the gap if $x \neq 0$. For the modes at Γ , there is no unit cell doubling, but the dispersion is different along X and Y , leading to an effective splitting of the VHS's, Figs. 9-10.

For the half-breathing mode we find that the softening is via the on-site Cu energy, Δ . Making Δ inequivalent on alternative rows of Cu's along the X -axis (parallel to the oxygen distortion) leads to a large splitting of the VHS's. Figure 8 shows that the gap is smaller than for the full breathing mode, but is clearly centered at the VHS.

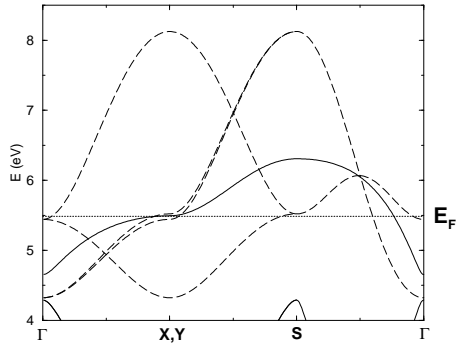


FIG. 10. Three-band dispersion of the CuO₂ planes, in the presence of a frozen ferroelectric (solid lines) or quadrupole mode (dashed lines) modulation, assuming $\beta/\alpha_d = 3.5$, and $\delta u/a = 0.08$.

B. Bond Stretching Modes in LSCO One-Band Model

To include electron-electron coupling, it is convenient to first reduce the above results to a one-band model. The parameters of the one-band model can readily be related to those of the three band model by expanding the approximate eigenvalues of Eq. 25 as $E_{i+} = \Delta_0 + W_i^2/\Delta_0$. In this way, it is found that the effective Cu-Cu hopping parameter is $t = t_0^2/\Delta_0$ [with the parameters assumed above, this would give $t = 0.42\text{eV}$, somewhat larger than the value 0.326eV estimated from photoemission], with phonon distortion parameters $\delta t/t = 2\delta t_0/t_0$ and $\bar{\delta}_1 = \delta_0 + \delta t$. Linearizing the results in δt_0 , it is readily seen that the flux dimer II mode has the symmetry of the conventional flux phase, and it is found that the quadrupole and ferroelectric modes do not couple at the one band level, while the breathing mode couples only via $\bar{\delta}_1$. The electronic dispersion can be solved:

$$E = -4t'c_xc_y \pm \sqrt{(m_1\bar{\delta}_1)^2 + |X_1 + X_2|^2}, \quad (26)$$

with m_1 and X_2 listed in Table III, and $X_1 = -2t(c_x + c_y)$. The result for the half breathing mode is distinct:

$$E = -2tc_y \pm \sqrt{(2\bar{\delta}_1 - 2\bar{\delta}tc_y)^2 + 4(t + 2t'c_y)^2c_x^2}. \quad (27)$$

The resulting dispersions are in excellent agreement with the corresponding antibonding band dispersions of the three band model.

For the half breathing mode the term in $\bar{\delta}t$ follows from the $\bar{\delta}_3$ term in Eq. 24: for a phonon distortion along X , the hopping along Y is modified along alternate rows, at $t \sim t_0^2/(\Delta_0 \pm \delta_3)$. Such a term has been previously considered by Shen, et al.¹⁸. In the present comparisons of different modes, the role of such a term has been neglected (by setting $\bar{\delta}_3 = 0$).

Table III: One Band Model Parameters

Mode	m_1	X_2	$\omega(\text{meV})$	$A(\text{eV})$
1. Breathing	4	0	66	60.4
2. Half-Breathing	2	-	83	47.8
3. Quadrupolar	0	0	56	43.5
4. Dimer I	0	$-2i\delta ts_x$	38	39.7
5. Dimer II	0	$-2i\delta t(s_x + s_y)$	38	79.5
6. Dimer III	0	$-2i\delta t(s_x - s_y)$	38	79.5
7. Shear	0	$-2\delta t(c_x - c_y)$	-	59
8. Ferroelectric	0	0	77	32.8
9. Flux Dimer I	0	$-2i\delta tc_x$	38	39.7
10. Flux Dimer II	0	$-2i\delta t(c_x - c_y)$	38	79.5
11. Flux Dimer III	0	$-2i\delta t(c_x + c_y)$	38	79.5
12. Flux Shear	0	$+2i\delta t(s_x - s_y)$	-	59

V. RESULTS IN STRONG COUPLING LIMIT

A. Electron-Electron Coupling

In one-dimensional metals, the CDW instability involves both electron-electron and electron-phonon coupling. Here we show that the same is true in the present two-dimensional problem: electron-electron interaction actually dominates the electron-phonon coupling in the cuprates. A nearest neighbor Coulomb interaction V contributes to all three components of pseudospin, Eqns. 2-4⁷⁰; it is estimated⁸⁹ that $V \simeq 0.2 - 0.3eV$.

The electronic part of the Hamiltonian can be written $H = H_{el} + H_1$ where the electronic kinetic energy is

$$H_{el} = \begin{pmatrix} E_1 & E_0 \\ E_0 & E_1 \end{pmatrix}, \quad (28)$$

with $E_0 = -2t(c_x + c_y)$, $E_1 = -4t'c_x c_y$, and t (t') is the (next) nearest neighbor hopping parameter. At mean field, the effects of both V and the on-site Coulomb interaction U can be included, leading to the Hamiltonian matrix

$$\begin{pmatrix} R_{z\sigma} + E_1 & E_0 + R_x + iR_y \\ E_0 + R_x - iR_y & -R_{z,\sigma} + E_1 \end{pmatrix}, \quad (29)$$

with eigenvalues

$$E_{\pm,\sigma} = E_1 \pm \sqrt{R^2 + E_0^2 + 2R_x E_0}, \quad (30)$$

where $R^2 = R_x^2 + R_y^2 + R_{z,\sigma}^2$, Fig. 11. In Eqns. 29,30, we take $R_x = R_{x0}\tilde{\gamma}$, $R_y = R_{y0}\tilde{\gamma}$, and $R_{z,\sigma} = R_{z0} + \sigma U m_z$, where the R_{i0} 's are constants, $\sigma = \pm 1$ is the spin, and m_z is the average magnetization per site in the antiferromagnetic phase induced by U . Parameter values are given in Section IIIA. The conventional⁶ flux phase dispersion is recovered from Eq.30 for the special choice of parameters: $t' = R_{x0} = R_{z,\sigma} = 0$ and $R_{y0} = 2t$ (compare Eq. 8).

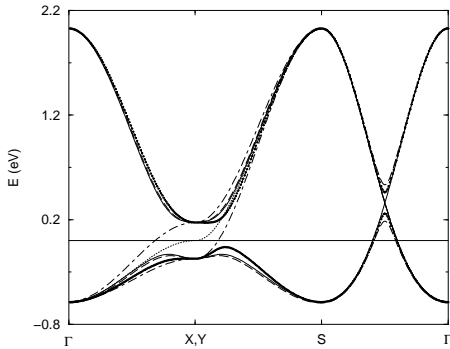


FIG. 11. Energy dispersion in the presence of pseudospin ordering, Eq. 30, for $t = 0.326eV$, $t' = -0.276t$, and $R_{x0} = R_{y0} = R_{z0} = 0.1eV$ (short dashed line); or $R_{i0} = 0.1732eV$ and the other two R 's = 0, for $i = x$ (dot-dashed line), y (solid line), or z (long dashed line); or all R_i 's = 0 (dotted line).

Note that while the interaction H_1 resembles H_{vib} of Eq. 27, there are a number of differences. First, while the term involving T_y is generated dynamically in the molecular problem, here a term in R_y appears explicitly. On a single plaquette, the three solutions are degenerate (the eigenvalues depend only on R , and not on the individual R_i 's), but intercell hopping and k -dependent coupling lead to slight dependence of the dispersion on the individual R_{i0} 's. (Note that R_x simply renormalizes t to have unequal values in the x and y directions. The effects of this term have been recently analyzed^{45,46}.) The solutions remain degenerate at the VHS, for equal R_{i0} 's.

Introducing the polarization

$$\Pi_{\vec{k},\sigma} = -\frac{f(E_{+,\sigma}) - f(E_{-,\sigma})}{E_{+,\sigma} - E_{-,\sigma}}, \quad (31)$$

the gap equations can be written

$$\sum_{\sigma} \int_{\vec{k}} \Pi_{\vec{k},\sigma} \Lambda_i = 1, \quad (32)$$

for i including all the non-vanishing gap contributions. The most general case has all four gap parameters, $R_{x0}, R_{y0}, R_{z0}, m_z$, nonvanishing, with corresponding $\Lambda_1 = \lambda_1(\tilde{\gamma} + E_0/R_{x0})\tilde{\gamma}$, $\Lambda_2 = \lambda_2\tilde{\gamma}^2$, $\Lambda_3 = \lambda_3(R_{z,\sigma}/R_{z0})$, and $\Lambda_4 = \lambda_4(1 + \sigma R_{z0}/U m_z)$. For the extended Hubbard model, the λ 's are⁷⁰: $\lambda_1 = \lambda_2 = 8V$, $\lambda_3 = 16V - 2U$, and $\lambda_4 = 2U$. (In the areas of overlap, these gap equations agree with those found by Nayak⁹⁰. However, a strong coupling calculation⁹¹ has suggested that only an attractive near-neighbor coupling would stabilize the flux phase.)

In the absence of on-site U , the near-neighbor interaction V favors the CDW, R_z . The energy lowering is exactly twice that of the other components, the factor of two arising from spin (since the x and y terms involve hopping, only terms with the same spin on both neighbors contribute; the z term has no such limitation). This is counteracted by strong coupling effects, since the CDW involves an imbalance of Cu site occupancies. Approximating $V = t$, $U = 6t$, $8V > 16V - 2U$, favoring the flux and shear phases. Because the couplings are not symmetrical (Eq. 30), these modes have slightly different gaps, $R_{x0} = 340meV$, $R_{y0} = 320meV$, $R_{z0} = 8.4meV$. However, $2U > 8V$, so in a purely electronic model the antiferromagnetic phase dominates, both at half filling and in the doped case. In the following subsections, it will be shown that electron-phonon coupling can reverse this situation in the doped cuprates, and also brings the CDW energy closer to that of the other phases.

B. Electron-Phonon Coupling

Combining the above results with electron-phonon coupling, we limit discussion to the three modes of primary interest. In the one-band model, the linear

electron-phonon coupling has exactly the same form as the V electron-electron term in Eq. 29. Thus, the free energy F is a function only of the *sums* of the electron-electron and electron-phonon gaps, leading to a simplification of the gap equations. For example, for the CDW $F = F(R_{z0} + 4\delta_1)$, so

$$\left\langle \frac{\partial F}{\partial \delta_1} \right\rangle = 4 \left\langle \frac{\partial F}{\partial R_{z0}} \right\rangle. \quad (33)$$

Since the averages are just those evaluated in the gap equations, they can be replaced by the derivatives of the quadratic terms, yielding:

$$\frac{\delta_1}{R_{z0}} = \frac{8\alpha_d^2 \Delta_0^2}{A(16V - 2U)} \simeq 0.22 \quad (34)$$

for $\alpha_d = 0.5$ and the other parameters as given above. For the shear mode, the equivalent result is

$$\frac{\delta t}{R_{x0}} = \frac{\beta^2 t^2}{AV} \simeq 0.068, \quad (35)$$

with $\alpha_t = 1$; an identical result holds for the flux phase, with appropriate A , yielding $\delta t/R_{y0} \simeq 0.05$. These are the analogs to Eq. 13. They are weak coupling results and should be modified when the gaps become comparable to the phonon frequencies. Thus, (1) there is substantial phonon coupling, but the transitions appear to be predominantly electronically driven; (2) the largest correction is for the CDW mode, although the correction is not large enough to make the CDW as unstable as the other two modes (if α_d were twice as large as estimated, all three modes would be approximately degenerate). Finally, (3) near half filling the corrections are not large enough to make any of the structural anomalies competitive with the AFM instability. This result is consistent with the finding of Hsu, et al.⁹², that the flux phase is unstable against magnetic order near half filling. It remains possible that additional couplings could tip the balance toward structural distortions, particularly in the doped materials. Certainly, there are strong indications of deviations from Migdal theory⁹³, and earlier calculations of the LTO and LTT instabilities found strong nonlinearities^{79,14}. In the following subsection we explore another possibility, a particular form of correlated hopping.

C. Unconventional Coupling Associated with O^{2-}

The O^{2-} ion is known to be inherently unstable, being stabilized in a solid by the Madelung potential of surrounding ions. This near instability has been suggested to be a driving force in ferroelectric transitions⁹⁴ in perovskites and in cuprate superconductivity⁹⁵. One of the principal manifestations of this near instability is the large change in ionic radius on doping O^{2-} to O^- .³⁵

While this anomaly should affect the electronic properties in a number of ways, we will here explore only one aspect, a correlated hopping.

When a hole is *localized* on a single oxygen, the shrinkage of its radius allows the adjacent coppers to approach much more closely. This would enhance the corresponding hopping probability, t , except that the presence of the hole inhibits other holes from hopping to the same site. If, however, the first hole hops away, it will take the local lattice some time to relax back, and in that interval there will be an enhanced probability of another hole hopping onto the oxygen. In a one band model, this would correspond to correlated hopping between adjacent Zhang-Rice singlets, or effectively, between adjacent coppers. This hopping adds a term

$$H_{c.h.} = -t_{c1} \sum_{\langle i,j \rangle, \langle i',j' \rangle, i \neq i'} c_{i\sigma}^\dagger c_{j\sigma} c_{j'\sigma'}^\dagger c_{i'\sigma'} \quad (36)$$

to the Hamiltonian. Such a term has been considered by Nayak⁹⁰; for related models, see Hirsch and Marsiglio⁹⁶. This term contributes $96t_{c1}$ to all three coupling parameters λ_i , $i = 1, 3$. From the present considerations, a value $t_{c1} = -2x\beta_{loc}\beta t\delta u_0/a \sim xt$ can be estimated, where $\delta u_0 \sim -0.3\text{\AA}$ is the shrinkage in radius³⁵ on going from O^{2-} to O^- . The factor x arises because holes only move preferentially onto the oxygens for doping beyond half filling, $x > 0$, while $\beta_{loc} \leq 1$ is a parameter introduced to describe the degree of localization of the hole on a single oxygen – predominantly due to polaronic effects. This factor is related to the delicate issue of the crossover from ionic to covalent behavior: $\beta_{loc} = 1$ corresponds to the ionic limit. The t_{c1} correction is so large that even a significantly covalent correction $\beta_{loc} < 1$ would allow the structural distortions to overcome the AFM state – but only for $x > 0$.

D. Numerical Results

Here we describe our numerical results. The gap equations follow from minimizing the mean-field free energy

$$F = \sum_{k,i=\pm} E_i f(E_i) - TS + Nf_0, \quad (37)$$

where S is the entropy, N the total number of electrons, and

$$f_0 = \frac{R_{x0}^2 + R_{y0}^2}{4V} + \frac{R_{z0}^2}{8V - U} + \sum_{i=1,3} A_i \left(\frac{\delta u_i}{a} \right)^2 + U(m_q^2 + \frac{x^2}{4}). \quad (38)$$

The E_i are solutions of Eq. 30 with phonon coupling included by the substitutions: $R_{z0} \rightarrow R_{z0} + 4\delta_1$, $R_{i0} \rightarrow R_{i0} + 2\delta t$, $i = x, y$. In Figure 12 we gradually turn on the phonon coupling, by varying the α factors from zero (no phonon coupling) to 1, covering the expected range

of coupling. Here we study the coupling near the VHS, $x = 0.25$. What is plotted is the self-consistent condensation energy. For weak phonon coupling, the CDW has the weakest coupling, due to the on-site Coulomb repulsion. However, it has the strongest intrinsic coupling to phonons, so as α_d is increased, it grows fastest, and can actually cross the other modes. The dotted line is the energy of the simple doped antiferromagnet (also at $x = 0.25$). It can be seen that for reasonable phonon coupling, the ground state is paramagnetic. The dashed lines show that even moderate correlated hopping ($\beta_{loc} = 0.1$) significantly enhances the binding energies, and shifts the degeneracy points of the CDW with the other modes to lower values of α .

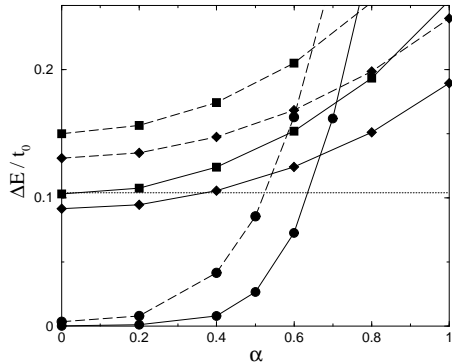


FIG. 12. Binding energy of various modes – site CDW (circles), bond CDW (squares) and flux phase (diamonds), for $\beta_{loc} = 0$ (solid lines) or 0.1 (dashed lines); horizontal dotted line = energy of doped antiferromagnetic phase. For all curves $x = 0.25$.

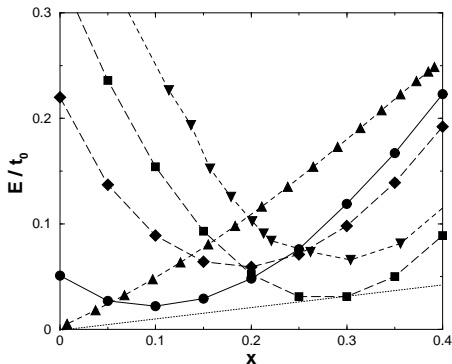


FIG. 13. Doping dependence of binding energies of phonon modes: site CDW (circles), bond CDW (squares), and flux phase (diamonds), assuming all mode α 's = 0.6, and $\beta_{loc} = 0.1(x/0.25)$. Also shown is the doped antiferromagnet (triangles) and ferromagnet (inverted triangles) [97]. The dotted line is the tangent construction for phase separation. For convenience in viewing, an energy shift $\delta E = 2.1(1-x)t_0$ has been added to all curves.

In Fig. 13 the doping dependence of the binding energies is illustrated for a representative $\alpha_i = 0.6$ ($i = d, t$), compared to that of the doped antiferromagnet and ferromagnet⁹⁷. All three CDW modes have a parabolic binding energy vs doping: for the bond-CDW and flux modes, the energy minima are near the VHS doping, while the site-CDW minimum is shifted to lower doping by the frustration effect discussed above (the minimum is no longer at $x = 0$, due to the strong correlation effect). A by now familiar^{17,98} Van Hove induced phase separation could arise between the antiferromagnetic insulator at half filling and *any* of the CDW modes. For the present parameter values, the lowest energy state involves the bond CDW at $x \sim 0.27$. Note in particular that the bond CDW is more stable than the ferromagnetic phase⁹⁷. This is consistent with the numerical results of Yonemitsu, et al.⁸⁷, who found a crossover from magnetic to dielectric polarons in the low doping regime. Remarkably, all three CDW curves approximately converge (weak JT degeneracy) at a doping, $x \sim 0.21$, close to the VHS. However, this crossover point is not directly observable, due to the phase separation. At this time we have not made a detailed study of the parameter dependence of these results, but the bond-CDW appears to be most stable. In particular, (1) α_d should probably be less than α_t ; and (2) our estimate for V may be a little large, but t_{c1} is probably too small, so V can be reduced and t_{c1} increased to keep a fixed coupling to the shear mode. Both of these corrections would act to further weaken the site-CDW. The results are quite intriguing. For a reasonable estimate of the parameters there is phase separation between the antiferromagnetic insulator and a paramagnetic state associated with LTT-like distortions, while the CDW and flux phase states are close in energy.

These results are in good agreement with the numerical calculations of Yonemitsu, et al.⁸⁷. In their work V was not included, so their phonon anomalies are of the breathing mode type, but they see clear evidence for nanoscale phase separation between antiferromagnetic background and dielectric polarons.

The present approach of turning on the electron-phonon interaction last (Fig. 12) makes the resulting near-degeneracy seem rather accidental. It is more natural to reexpress the result: for *both* electron-electron and electron-phonon coupling, the flux and bond-CDW phases are nearly degenerate, while the site-CDW is more strongly coupled. However, the on-site Coulomb repulsion opposes site-CDW formation, making the three modes nearly degenerate in energy.

VI. DISCUSSION: FUTURE DIRECTIONS

The present paper establishes the framework for analyzing CDW's in the cuprates, and Berryonic matter in a number of related materials. Clearly much work remains to be done. This includes:

VII. CONCLUSIONS

(1) From the associated susceptibilities the modifications to the electronic dispersion can be calculated and compared with the kink^{32,33} seen in photoemission. While phononic contributions appear to be important¹⁸, Valla⁹⁹ has noted that the linear frequency dependence of the imaginary self energy extends to much too high frequencies to be solely due to strong electron-phonon coupling. This is consistent with the present results, that the CDW has a strong electron-electron component. Hence, both components will be important in interpreting the photoemission dispersion, with proximity to a VHS providing a marginal Fermi liquid-like¹⁰⁰ background and phonon coupling the kink in the dispersion.

(2) The manner in which the y -component couples to the Hamiltonian is markedly different in the molecular and lattice versions of the theory: in the molecular version, the direct electron-phonon coupling is to the x and z components (B_1 and B_2 modes), with the dJT term generated dynamically – from the phonon kinetic energy term. In the lattice, the flux phase term arises directly from electron-electron coupling via V , and corresponding terms are allowed in the Hartree-Fock expansion of the electron-phonon coupling. It remains to be seen what role phonon kinetic energy plays in the lattice problem. [One effect will presumably be the kink in the electronic dispersion when $E = \hbar\omega_{ph}$.]

(3) Fluctuations of the CDW's (or of the stripes) should appear as new low frequency (or pinned) phonon modes⁷⁵. It is possible that such modes have been observed in microwave measurements.¹⁰¹

(4) It remains to work out the detailed doping dependence, in terms of stripes.

(5) It will be important to provide detailed calculations showing how the shear mode couples to the various bond bending modes in the different cuprates. A related issue: are there tilt distortions in the flux phase? (if so, then experimental evidence for local LTT order could really be associated with the flux phase.)

(6) One puzzling feature is the role of the LTO phase. Near optimal doping it would seem to be predominantly associated with local LTT order, but it seems to be a uniform phase near half filling. In principle, its presence could be accidental, particularly since it is only present in LSCO, but it does provide an easy axis for orienting the spins, and hence may be involved in the stripe crossover from vertical to diagonal. (Also, the pseudogap seems to follow $T_{pg}(x) = 2T_{LTO}$.²⁹)

(7) A very similar model should apply to the nickelates, and extensions can be made to other forms of Berryonic matter.

(8) There remains the problem of the competition of density wave order with superconductivity, and the possible roles of magnetic fluctuations.

This results of this paper have bearings on four separate issues. First, on a purely formal level, the paper presents an alternative approach (phonon flux phases) to the dJT effect in solids, revealing previously unsuspected analogies between flux phases and Berryonic matter. Secondly, The approach is applied to the cuprates, which are an *a priori* unlikely candidate for JT effects. Nevertheless, a ‘hidden’ JT degeneracy is found, and a numerical estimate suggests that the cuprates are close to the weak degeneracy point of a square molecule, which should enhance the possibility of a dynamic flux phase. These calculations can be considered a generalization of the results of Yonemitsu, et al.⁸⁷, by (a) reducing the problem to a one band model, (b) including a nearest neighbor Coulomb repulsion which enhances the scope of CDW-like instabilities, and (c) providing a mean-field underpinning for the numerical calculations of local electronic phase separation. Third, the paper explores the relative strength of different CDW-like distortions in the cuprates, and suggests an explanation for strong coupling to the LTT and half-breathing modes. The role of these distortions in stabilizing charged stripes is discussed in an Appendix. Finally, the results offer strong support for the general picture of stripe phases as stabilized by VHS-induced ordering. A similar approach should be applicable to other systems, and in particular, to nickelates where the coupling to the CDW/breathing mode is known to be stronger.

For the cuprates, we find that the structural distortions are close to the dJT degeneracy, but that the shear and flux phases are more unstable than the CDW. Hence, one would expect significant softening of the breathing modes, but instability in either the shear or flux phases. These expectations are borne out in experiments on the cuprates, with the shear mode coupling to a (local) LTT order. The near degeneracy of the shear and flux phases is consistent with experimental evidence for both modes. Perhaps the most interesting phase is the flux phase, which is closely related to a chaotic dJT phase.

Recently, dJT phases have been proposed in a number of exotic materials, including cuprates¹⁵, buckyballs¹² and manganates¹⁶. To describe the dJT phase of buckyballs, the concept of Berryonic matter was introduced⁵. In this model, no attempt was made to accurately model Buckyball solids. Instead, a lattice of dJT molecules was assumed, basing their properties on the known anomalies associated with triatomic molecules. Since the square molecule, Fig. 2, has the same dJT anomaly as the triangular model when $E_{JT}^1 = E_{JT}^2$, and this degeneracy persists on a square lattice (Section IIIC), the present model should be an excellent starting point for studies of Berryonic matter. Moreover, the proximity of the cuprates to the Berryonic limit should stimulate interest in this unusual state of matter.

APPENDIX A: PHONONS ON STRIPES

In the Van Hove model, charged stripes (or domains) are stabilized at a particular density by a VHS driven ordering instability, most likely a CDW¹⁷ as analyzed here. Originally, this distinguished the VHS stripe model from magnetic models, in which the charged stripes were structureless domain walls between antiferromagnetic domains. However, in 1995, it was found¹⁰² that the hole density on the charged stripes in LSCO:Nd is considerably less than one per copper, and the magnetic models were modified to include CDW order on the charged stripes¹⁰³. The form of CDW order proposed generally differs from that discussed here (being more one-dimensional), and the models still do not explain the experimental observation that charge ordering arises at higher temperatures than spin ordering. Here we discuss experimental evidence linking the phonon anomalies specifically to charged stripes. It should be noted that there must in general be a coupling to all modes: the charge modulation will act to scatter all phonons; here we are speaking of a stronger coupling, with phonons localized on the stripes.

It is by now clear that the LTT phase plays an important role in stabilizing a nearly static stripe phase¹⁰² in $\text{La}_{2-x-y}\text{R}_y\text{A}_x\text{CuO}_4$ (LACO:R) with R a rare earth (RE), typically Nd or Eu , and $A = \text{Sr}, \text{Ba}, \text{or Ca}$. The reasons for this stabilization are less clear. One explanation¹⁰² is a simple pinning effect: the stripes ‘prefer’ to run parallel to the Cu-O-Cu bonds, and the LTT distortions lock them into an ordered array. However, it is not necessarily true that LTT order enhances stripe pinning: in Eu substituted samples, the Cu spins appear to be even more dynamic in the LTT phase¹⁰⁴. Moreover, such a picture completely fails to explain the common occurrence of *simultaneous* fluctuating stripe order and fluctuating LTT order. States with fluctuating local order are relatively uncommon, and for two dynamic phases to appear simultaneously and to interact strongly, but to have completely independent origins stretches credulity. It is much more likely that the connection is fundamental: that the structural and stripe orders are two aspects of a single phenomenon. Indeed, this must be the case: neutrons are insensitive to individual electrons, so the neutron diffraction evidence for long range stripe order¹⁰² is really detecting an accompanying structural order. Perhaps part of the problem is a limited vocabulary for dealing with fluctuating local structural order: the *average macroscopic* structure will generally appear to be LTO or LTT or some intermediate structure; only if the domains are of sufficiently large scale would one expect to see a clear mixture of two phases.

Hence, this Appendix deals specifically with evidence that the structural order is also short range, and evolves with doping in parallel with the electronic stripes. The cumulative evidence supports a picture of coexisting structural and electronic stripe structure: whenever

stripes are present, not only are the electronic properties inhomogeneous (with insulating magnetic and conducting charged stripes), but also the lattice distortions, with local LTT distortions on the charged stripes, while low-temperature orthorhombic (LTO) distortions are favored by the magnetic stripes. This strongly supports a model of the stripe phase as a form of nanoscale phase separation, with the charged-stripe phase stabilized by an LTT-like phase^{14,15}.

1. Coupling of Charged Stripes to local LTT Order

a. LTT-LTO Competition

Uniform, macroscopic LTT order is rare in the $\text{La}_{2-x}\text{Sr}_x\text{CuO}_4$ (LSCO) family of cuprates. There is a narrow regime of LTT phase near optimal doping in $\text{La}_{2-x}\text{Ba}_x\text{CuO}_4$ (LBCO), while long-range LTT order can only be induced in LSCO by replacing some La with a RE, typically Nd or Eu . However, *short range* LTT order appears to be more pervasive.

EXAFS measurements by Bianconi and coworkers found evidence for anomalous long Cu-O bonds in doped $\text{Ba}_2\text{Sr}_2\text{CaCu}_2\text{O}_8$ (BSCCO)¹⁰⁵ and LSCO³⁹, which were interpreted in terms of stripes with alternating LTO-LTT orders. A number of experiments⁴⁰⁻⁴⁴ have explored the possibility¹⁵ that the high-temperature tetragonal (HTT) and LTO phases can be ‘dynamic LTT’ phases (i.e., with local LTT order). Billinge, et al.⁴⁰ analyzed neutron diffraction pair distribution functions (PDF’s) of LBCO, and found that in the LTO phase the local order has LTT symmetry, crossing over to average LTO structure on a 10\AA length scale. Moreover, there is no change in the local structure when warming into the HTT phase. EXAFS results are consistent⁴¹. In LSCO, Božin, et al.^{43,44} find a crossover from local LTO order very near half filling, to a clear mixing of local LTO and LTT order in the doped materials. The results are influenced by large local distortions near the dopants, particularly in LBCO associated with the large difference in ionic size between Ba^{+2} and La^{+3} ,⁴¹ but also near the dopant Sr sites⁴². It has been suggested¹⁰⁶ that the distortions are characteristic of the hole-doped CuO_2 planes, but with enhanced distortion near Sr due to partial hole localization. These doped materials display considerable tilt and bond-length disorder, interpretable in terms of stripes.

A crossover from local LTO to local LTT order with increased doping is an intriguing possibility, particularly in light of the crossover in *stripe orientation* from diagonal at low doping¹⁰⁷, which could be ‘pinned’ by LTO order, to horizontal near optimal doping. (It has been suggested that the LTT distortions orient the stripes along the Cu-O bonds¹⁰⁸.) The connection between the LTO phase and magnetic stripes may be related to strong magnetoelastic coupling: in the Néel phase, the spin flop transition is strongly suppressed by LTT order¹⁰⁴, while in the diag-

onal stripe phase the cluster spin glass transition can be seen in anelastic relaxation measurements¹⁰⁹. The Mott insulator $\text{Sr}_2\text{CuO}_2\text{Cl}_2$ (SCOC) is found by x-rays to be tetragonal, but below the Néel temperature the infrared absorption peak associated with the Cu-O bending mode phonon is found to split into two components¹¹⁰.

b. LTT and Stripes

Recent studies have added considerable evidence for direct phonon coupling to stripes. First, of course, is the direct neutron diffraction evidence for charge order^{102,54}: what is seen by neutrons is not the electronic charges themselves, but an accompanying lattice distortion, suggesting that the distortion is a fundamental part of the stripes. These anomalies, and related anomalies of the half-breathing mode²⁰ need not imply that stripes are stabilized by electron-phonon coupling¹⁷: it could simply be that there is stronger electron-phonon coupling on hole-doped stripes. On the other hand, Bianconi, et al.²⁵ report EXAFS evidence for a quantum critical point (QCP) – a local splitting of the Cu-O bond length which can be tuned to zero by adjusting the chemical microstrain. It is found that the highest critical temperatures are associated with this optimal degree of ‘microstrain’²⁵. The associated bondlength splittings are much larger than can be accounted for by the doping dependence of the average lattice constant, and hence point to a structural QCP distinct from stripe formation. Finally, there is the finding⁴⁴ that local LTT-LTO type structural disorder is characteristic of the stripe regime, and the structural disorder greatly reduces near $x = 0.25$, close to the point where the stripe phase terminates^{111,112}. This near coincidence of stripe disorder and structural disorder provides very strong evidence that the two kinds of stripe are associated with two kinds of structural order: that the LTO phase is connected with magnetic stripes, at half filling, and the LTT phase with charged stripes, near optimal doping. The data *cannot* be understood in terms of preexisting stripes accidentally pinned by a uniform LTT order.

Thermal conductivity measurements suggest a very close connection between stripe order and the LTT phase. Thermal conductivity κ has proven to be an important probe of the charge ordering transition in nickelates and manganites¹¹³. Typically, κ is suppressed above the transition due to collisions between phonons and fluctuating stripes. Baberski, et al.¹¹⁴ find a very similar suppression of κ in the cuprates, but *always at the LTT transition*. Figure 14 compares the thermal conductivity near the LTT transition in LSCO:Nd [114] (b) with that of the charge ordering transition in a manganite¹¹⁵ (a), suggesting an intimate connection between the LTT and charge ordering transitions. In the absence of long range LTT order, κ is suppressed over the full temperature range – this is found both for pure LSCO and for the RE substi-

tuted materials, for $x > 0.17$. The thermal conductivity suppression persists down to the lowest doping studied, $x = 0.05$, and the jump at T_{LTT} actually increases with decreasing x . However, suppression is absent in the undoped materials. It would be most interesting to see if the suppression terminates near $x = 0.05$, where there is a superconductor-insulator transition and the stripes cross over from horizontal to diagonal.

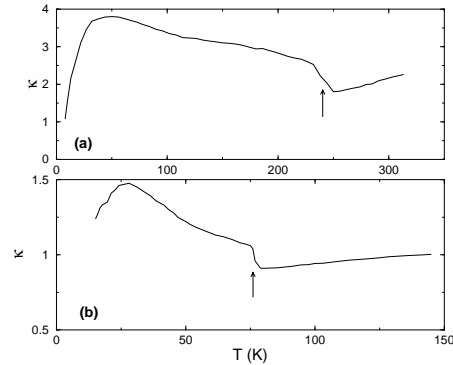


FIG. 14. Thermal conductivity of (a) $\text{La}_{0.525}\text{Pr}_{0.1}\text{Ca}_{0.375}\text{MnO}_3$ [115], and (b) $\text{La}_{1.28}\text{Nd}_{0.60}\text{Sr}_{0.12}\text{CuO}_4$ [114].

The close connection between the LTT phase and charged stripes is further illustrated by a recent study of the rich phase diagram found^{116,117} in $\text{La}_{1.6-x}\text{Nd}_{0.40}\text{Sr}_x\text{CuO}_4$, Fig. 15a. This complex behavior can be simply understood (Fig. 15b) if it is kept in mind that the structural phases are macroscopic averages, while local structure can be more complicated. We assume that the LTO phase is associated both with the high-temperature electronically disordered phase, and with the magnetically ordered phase at $x = 0$, while the LTT phase is characteristic of hole-doped stripes. As temperature is decreased, long-range stripe order arises in two steps: first the charges order (filled circles) then the spins (dot-dashed line). The other curves in the diagram are associated with fluctuating stripe order. Thus, the NQR ‘knockout’ line may indicate the onset of stripe fluctuations¹¹⁷; at nearly the same phase boundary XANES¹¹⁸ and PDF⁴⁴ measurements find the onset of local Cu-O bondlength variations suggestive of local LTT-type tilts. Near 1/8 doping (vertical line) there is a crossover in the stripe fluctuations: at low doping there are narrow charged stripes fluctuating in a magnetic (LTO) background; at higher doping narrow magnetic stripes fluctuate in a charged (LTT) background. Long range charge order (filled circles) coincides with the *lower* of the LTT(-like) transition or the NQR knockout line.

Magnetic field studies provide additional evidence. The Hall effect¹¹⁹ in strongly Nd substituted LSCO shows a crossover from one-dimensional ($R_H \rightarrow 0$ as $T \rightarrow 0$) to two-dimensional behavior at $x = 0.12$; for $x < 0.12$, the R_H anomaly turns on with stripe order

– exactly at the LTT-like phase transition. Further, it is known that an in-plane magnetic field has a strong effect on magnetoresistance, including hysteretic effects which can be interpreted as field-induced rotation of the stripes¹²⁰. Remarkably, an in-plane field also has a strong effect on the LTT-LTO transition temperature¹²¹, stabilizing the LTT phase at higher T . This can be qualitatively understood, if the LTT phase and charge stripes are intimately related: the fluctuating (LTT) stripes are present in the LTO phase, but the strong fluctuations produce an average LTO structural order; the field, by aligning the stripes, reduces transverse fluctuations and reveals the underlying LTT order.

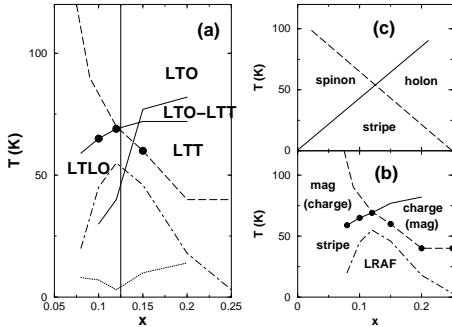


FIG. 15. (a) Phase diagram of $\text{La}_{1.6-x}\text{Nd}_{0.40}\text{Sr}_x\text{CuO}_4$ [116]. Solid lines = structural transitions, with various phases labelled (LTO-LTT = mixed phase, LTLO = low temperature less orthorhombic phase). Long dashed lines = NQR knock-out line [117], indicating onset of slow stripe fluctuations; circles = charge order; dot-dashed line = long-range (incommensurate) antiferromagnetic (LRAF) order; dotted line = superconductivity. (b) Interpretation, in terms of dominant and subdominant (in parentheses) fluctuations. (c) Spin-charge separation phase diagram [133]: below the dashed line spinons are paired, below the solid line holons are Bose condensed.

In summary, the data suggest the following scenario. The magnetic stripes are associated with a local LTO-type tilt distortion, the charged stripes with an LTT tilting. At half filling, there is a simple long-range LTO order, which may be stabilized by magnetoelastic coupling which aligns the spins with the LTO tilt direction. The LTT tilting, stabilized by coupling to the VHS, is fluctuating unless pinned by ionic disorder off of the CuO_2 planes. When the LTT phase is pinned, the stripes develop long-range charge (and ultimately spin) order. If the stripe pinning is strong enough, the superconducting order can be suppressed, predominantly due to the magnetic order¹¹⁶. Near enough to half filling, the LTO tilts prevail, the stripes rotate by 45° , and superconductivity is destroyed.

Thus there is a three-way competition, between magnetic, structural, and superconducting order. Such a model could explain why superconductivity is not found in the nickelates and manganites, where electron-phonon

coupling is stronger. The competition between superconductivity and LTT order takes place predominantly *on the charged stripes*^{112,29}, and is strongly influenced by interlayer strains, which can be varied by rare earth substitution. Büchner, et al.¹²² find a critical tilt angle Φ_c , such that when the average LTT tilt exceeds Φ_c , ‘bulk’ superconductivity is absent (the Meissner fraction is greatly reduced), while for tilts less than Φ_c superconductivity is hardly affected by the presence of LTT order. Experimentally, it is often found that when LTT fluctuations are weak (e.g., in some compositions of LSCO and oxygen-doped La_2CuO_4 ¹²³), magnetic order develops exactly at the superconducting transition. Julien, et al.¹²⁴ have suggested that magnetic fluctuations are present at much higher temperatures, and that the sudden slowing of the fluctuations at T_c is coincidental. We suggest a slightly different possibility: that when LTT pinning is particularly weak, it takes superconducting order to provide the stripe phase with structural rigidity, and that it is the stiffening of the charge stripes which is reflected in the slowing of the magnetic fluctuations. This provides one more demonstration that the charged stripes can be either superconducting or LTT ordered.

2. Flux Phase on Stripes

Early studies of the flux phase generally concentrated on the competition between the flux and antiferromagnetic phases at half filling. The present analysis strongly suggests that the flux phase would be present instead in the hole doped region – that is, on the charged stripes. This follows both because instability is enhanced near a VHS, and because the correlated hopping scales with x ; moreover, in a stripe picture, features near the Fermi level are generally associated with the charged stripes¹¹². This conclusion is consistent with the experimental observation¹⁹ that the possible flux related magnetization is stronger in YBCO_{6+y} for $y=0.6$ than for $y=0.35$ (see also Chakravarty, et al.¹²⁵). It also provides a natural resolution of the Lee-Wen paradox¹²⁶ discussed by Orenstein and Millis¹²⁷. Lee and Wen showed that they could explain the Uemura relation for underdoped cuprates, as long as the flux phase dispersion is independent of doping. The paradox is that many strong-coupling models expect the dispersion to renormalize to zero near the Mott insulator at half filling. In a stripe picture, this renormalization is taken as indicating that the *fraction of material* associated with charged stripes renormalizes to zero at half filling, whereas the *dispersion on a single stripe* is less sensitive to doping¹¹².

At very low doping, flux-strips will tend to break up into flux-polarons, confined to a single plaquette. These flux-polarons bear a close resemblance to the skyrmions introduced by Gooding¹²⁸. Indeed, his electronic states are just linear combinations of the E_u -symmetry plaquette states of Eq. 9. The difference is that his states are

localized around a Sr impurity, while ours are the equilibrium conducting state on the hole-doped stripes. Clearly, at low temperatures there will be a tendency for charged stripes and polarons to be pinned on the Sr, greatly enhancing the similarity. However, the present model more naturally explains stripes at higher doping levels, and the uniform charged phase near x_0 . It should be noted that Haskel, et al.⁴² find enhanced local structural distortions near Sr impurities, associated with hole localization¹⁰⁶.

If the flux phase is on the charged stripes, then hole doping will shift the Fermi level away from the conical points, producing not a node but a hole pocket, as in Fig. 11). It is possible that the deviations from d-wave symmetry found in the underdoped regime¹²⁹ are associated with this hole pocket. The apparent d-wave gap might then be a *localization* gap at the hole pocket Fermi surface, leading to the localization effects observed in resistivity^{130,131}.

3. Spinons and Holons and Stripes

Overall, the idea that stripes involve competition between antiferromagnetism, d-wave superconductivity, and the flux phase is very attractive, and arises naturally from an SO(6) symmetry (a subgroup of the SO(8) group⁶⁶), in which all three states comprise a single 6-dimensional order parameter, Fig. 16. In fact, in the repulsive Hubbard model at half filling, when $t' = 0$, there is an extra electron-hole symmetry, leading to a degeneracy between the flux phase and d-wave superconductivity (dSC)¹³². This is equivalent to the degeneracy between a CDW and s-wave superconductivity (sSC) in the attractive Hubbard model, since the flux phase is a form of d-wave CDW. In fact, the τ operator of Eq. 2 transforms the OAF and dSC operators into the CDW and sSC operators⁶⁶. This degeneracy is the basis for the SU(2) model of superconductivity¹²⁶. The SO(6) model thus encompasses the SO(5) and SU(2) models, Fig. 16.

There is a close similarity between the experimental doping dependence of LSCO, Fig. 15a,b and the spinon-holon phase diagram^{133,134}, Fig. 15c, with the spinon-condensed phase corresponding to the magnetic stripe dominated regime and the holon-condensed phase corresponding to the charged stripe dominated regime, as indicated by the experimental LTT phase, Fig. 15a! Strikingly, the holon condensed regime is where the holes have a flux-phase Fermi surface¹³⁴. Indeed, it would seem that spin-charge separation can be interpreted as a theory of stripe phase formation. Thus, the spinon pairing involves the exclusion of spin deviations from an antiferromagnetic domain onto an antiphase domain wall, while holon condensation involves the ordering which stabilizes the charged domains (the flux phase). The spin gap would then correspond to a quantum confinement energy¹¹². When both spinons and holons are condensed together, well-defined stripe order results. As early as

1987, Anderson¹³⁵ noted that spinon and holon condensation should couple to structural distortions. Superconducting order seems to be more characteristic of the holon condensed domain (charged stripes) than of the stripe phase regime.

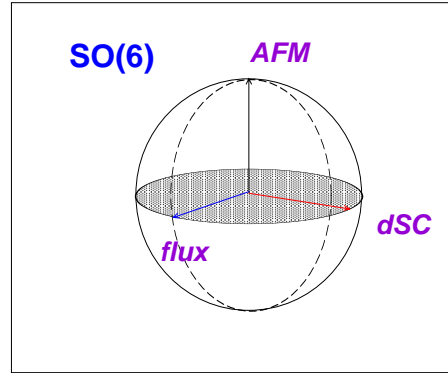


FIG. 16. Six dimensional order parameter in SO(6) theory [66], with three components of magnetic order (AFM), two of d-wave superconductivity (dSC), and one of flux phase (flux). In a stripe picture, the shaded plane would correspond to the charged stripes.

-
- ¹ G. Herzberg and H.C. Longuet-Higgins, Disc. Farad. Soc. **35**, 77 (1963).
 - ² H. von Busch, Vas Dev, H.-A. Eckel, S. Kasahara, J. Wang, W. Demtröder, P. Sebal, and W. Meyer, Phys. Rev. Lett. **81**, 4584 (1998).
 - ³ R. Englman and B. Halperin, Phys. Rev. **B2**, 75 (1970); B. Halperin and R. Englman, Phys. Rev. **B3**, 1698 (1971).
 - ⁴ I.B. Bersuker and V.Z. Polinger, “Vibronic Interactions in Molecules and Crystals” (Springer, Berlin, 1989).
 - ⁵ N. Manini, E. Tosatti, and S. Doniach, Phys. Rev. **B51**, 3731 (1995); G. Santoro, M. Airoidi, N. Manini, E. Tosatti, and A. Parola, Phys. Rev. Lett. **74**, 4039 (1995); D. Shelton and A.M. Tsvelik, unpublished.
 - ⁶ I. Affleck and J.B. Marston, Phys. Rev. **B37**, 3774 (1988).
 - ⁷ R.B. Laughlin, J. Phys. Chem. Sol. **56**, 1627 (1995); X.-G. Wen and P.A. Lee, Phys. Rev. Lett. **76**, 503 (1996).
 - ⁸ D.A. Ivanov, P.A. Lee, and X.-G. Wen, Phys. Rev. Lett. **84**, 3958 (2000); S. Chakravarty, R.B. Laughlin, D.K. Morr, and C. Nayak, Phys. Rev. **B63**, 94503 (2001); see also D.J. Scalapino and S.R. White, cond-mat/0007515.
 - ⁹ E. Cappelluti and R. Zeyher, Phys. Rev. **B59**, 6475 (1999).
 - ¹⁰ B.I. Halperin and T.M. Rice, in “Solid State Physics, Vol. 21”, ed. by F. Seitz, D. Turnbull, and H. Ehrenreich (Academic, N.Y., 1968), p. 115.
 - ¹¹ H.J. Schulz, Phys. Rev. **B39**, 2940 (1989).
 - ¹² C.M. Varma, J. Zaanen, and K. Raghavachari, Science **254**, 989 (1991); M. Lannoo, G.A. Baraff, M. Schlüter,

- and D. Tomanek, Phys. Rev. B**44**, 12106 (1991); M. Schlüter, M. Lannoo, M. Needels, G.A. Baraff, and D. Tománek, Phys. Rev. Lett. **68**, 526 (1992), and Mat. Sci. & Eng. B**19**, 129 (1993); V.P. Antropov, O. Gunnarsson, and A.I. Liechtenstein, Phys. Rev. B**48**, 7651 (1993); A. Auerbach, Phys. Rev. Lett. **72**, 2931 (1994).
- ¹³ K.A. Müller, J. Supercond, **12**, 3 (1999).
- ¹⁴ R.S. Markiewicz, Physica C**200**, 65 (1992).
- ¹⁵ R.S. Markiewicz, Physica C**210**, 235,264 (1993).
- ¹⁶ A.J. Millis, P.B. Littlewood, and B.I. Shraiman, Phys. Rev. Lett. **74**, 5144 (1995); A.J. Millis, B.I. Shraiman, and R. Mueller, Phys. Rev. Lett. **77**, 175 (1996); A.J. Millis, Phys. Rev. B**53**, 8434 (1996).
- ¹⁷ R.S. Markiewicz, J. Phys. Cond. Matt. **2**, 665 (1990).
- ¹⁸ A. Lanzara, P.V. Bogdanov, X.J. Zhou, S.A. Kellar, D.L. Feng, E.D. Lu, T. Yoshida, H. Eisaki, A. Fujimori, K. Kishio, J.-I. Shimoyama, T. Noda, S. Uchida, Z. Hussain, and Z.-X. Shen, cond-mat/0102227; Z.-X. Shen, A. Lanzara, and N. Nagaosa, cond-mat/0102244.
- ¹⁹ H. A. Mook, Pengcheng Dai, and F. Dogan, cond-mat/0102047.
- ²⁰ R.J. McQueeney, Y. Petrov, T. Egami, M. Yethiraj, G. Shirane, and Y. Endoh, Phys. Rev. Lett. **82**, 628 (1999).
- ²¹ Y. Petrov, T. Egami, R.J. McQueeney, M. Yethiraj, H.A. Mook, and F. Dogan, cond-mat/0003414.
- ²² R.J. McQueeney, J.L. Sarrao, P.G. Pagliuso, P.W. Stephens, and R. Osborn, cond-mat/0104118.
- ²³ R.J. McQueeney, J.L. Sarrao, J.S. Gardner, M.F. Hundley, and R. Osborn, Phys. Rev. B**60**, 80 (1999).
- ²⁴ L. Pintschovius and M. Braden, Phys. Rev. B**60**, 15039 (1999).
- ²⁵ A. Bianconi, G. Bianconi, S. Caprara, D. Di Castro, H. Oyanagi, and N.L. Saini, J. Phys. Cond. Matt. **12**, 10655 (2000).
- ²⁶ R.S. Markiewicz, Bull. A.P.S. **43**, 320 (1998), R.S. Markiewicz, C. Kusko, and M.T. Vaughn, *ibid.* **44**, 460 (1999).
- ²⁷ W. Weber, Phys. Rev. Lett. **58**, 1371 (1987).
- ²⁸ M. Grilli and C. Castellani, Phys. Rev. B**50**, 16880 (1994); F. Becca, M. Tarquini, M. Grilli, and C. di Castro, Phys. Rev. B**54**, 12443 (1996).
- ²⁹ R.S. Markiewicz, J. Phys. Chem. Sol. **58**, 1179 (1997).
- ³⁰ L. Pintschovius and W. Reichardt, in “Physical Properties of High Temperatures IV”, ed. by D.M. Ginsberg (World Scientific, Singapore, 1994), p. 295.
- ³¹ R.J. McQueeney, A.R. Bishop, Y.-S. Yi, and Z.G. Yu, J. Phys. Cond. Matt. **12**, L317 (2000); J. Tranquada, K. Nakajima, M. Braden, L. Pintschovius, W. Reichardt, and R. McQueeney, Bull. A.P.S. **46**, 1115 (2001).
- ³² P.V. Bogdanov, A. Lanzara, S.A. Kellar, X.J. Zhou, E.D. Lu, W. Zheng, G. Gu, K. Kishio, J.-I. Shimoyama, Z. Hussain, and Z.X. Shen, Phys. Rev. Lett. **85**, 2581 (2000).
- ³³ A. Kaminski, M. Randeria, J.C. Campuzano, M.R. Norman, H. Fretwell, J. Mesot, T. Sato, T. Takahashi, and K. Kadowaki, Phys. Rev. Lett. **86**, 1070 (2001).
- ³⁴ N.W. Ashcroft and N.D. Mermin, “Solid State Physics” (Saunders, Fort Worth, 1976), p. 519.
- ³⁵ R.S. Markiewicz, Physica C**255**, 211 (1995).
- ³⁶ M. Nohara, T. Suzuki, Y. Maeno, T. Fujita, I. Tanaka, and H. Kojima, Phys. Rev. Lett. **70**, 3447 (1993); S. Sakita, T. Suzuki, F. Nakamura, M. Nohara, Y. Maeno, and T. Fujita, Physica B**219-220**, 216 (1996).
- ³⁷ M. Braden, W. Paulus, A. Cousson, P. Vigoureux, G. Heger, A. Goukassov, P. Bourges, and D. Petitgrand, Europhys. Lett. **25**, 625 (1994); M. Braden, P. Adelman, W. Paulus, P. Vigoureux, G. André, P. Schweiss, A. Cousson, A. Goukassov, S.N. Barilo, D.I. Zhigounov, and G. Heger, Physica C**235-240**, 793 (1994).
- ³⁸ T. Egami and S.J.L. Billinge, in “Phys. Props. of High T. Superconductors V”, ed. by D.M. Ginsberg (World Scientific, Singapore, 1996).
- ³⁹ A. Bianconi N.L. Saini, A. Lanzara, M. Missori, T. Rosetti, H. Oyanagi, H. Yamaguchi, K. Oka, and T. Ito, Sol. St. Commun. **76**, 3412 (1996).
- ⁴⁰ S.J.L. Billinge, G.H. Kwei, and H. Takagi, Phys. Rev. Lett. **72**, 2282 (1994).
- ⁴¹ D. Haskel, E.A. Stern, F. Dogan, and A.R. Moodenbaugh, Phys. Rev. B**61**, 7055 (2000).
- ⁴² D. Haskel, E.A. Stern, D.G. Hinks, A.W. Mitchell, J.D. Jorgensen, and J.I. Budnick, Phys. Rev. Lett. **76**, 439 (1996); D. Haskel, E.A. Stern, D.G. Hinks, A.W. Mitchell, and J.D. Jorgensen, Phys. Rev. B**56**, 521 (1997).
- ⁴³ E.S. Božin, S.J.L. Billinge, G.H. Kwei, and H. Takagi, Phys. Rev. B**59**, 4445 (1999).
- ⁴⁴ E.S. Božin, G.H. Kwei, H. Takagi, and S.J.L. Billinge, Phys. Rev. Lett. **84**, 5856 (2000), M. Gutmann, E.S. Božin, and S.J.L. Billinge, cond-mat/0009141.
- ⁴⁵ C.J. Halboth and W. Metzner, Phys. Rev. Lett. **85**, 5162 (2000).
- ⁴⁶ B. Valenzuela and M.A.H. Vozmediano, Phys. Rev. B**63**, 153103 (2001).
- ⁴⁷ A.P. Giddy, M.T. Dove, G.S. Pawley, and V. Heine, Acta Cryst. A**49**, 697 (1993); M.T. Dove, V. Heine, and K.D. Hammonds, Mineralogical Mag. **59**, 629 (1995).
- ⁴⁸ P. Schweiss, W. Reichardt, M. Braden, G. Collin, G. Heger, H. Claus, and A. Erb, Phys. Rev. B**49**, 1387 (1994).
- ⁴⁹ J. Röhler, Physica B**284-88**, 1041 (2000).
- ⁵⁰ O.K. Andersen, A.I. Liechtenstein, O. Rodriguez, I.I. Mazin, O. Jepsen, V.P. Antropov, O. Gunnarson, and S. Gopalan, Physica C**185-189**, 147 (1991).
- ⁵¹ V. Pasler, P. Schweiss, C. Meingast, B. Obst, H. Wühl, A.I. Rykov, and S. Tajima, Phys. Rev. Lett. **81**, 1094 (1998).
- ⁵² E. Kaldis, J. Röhler, E. Liarokapis, N. Poulakis, K. Conder, and P.W. Loeffen, Phys. Rev. Lett. **79**, 4894 (1997).
- ⁵³ M.C. Schnabel, C.-H. Park, A. Matsuura, Z.-X. Shen, D.A. Bonn, R. Liang, and W.N. Hardy, Phys. Rev. B**57**, 6090, 6107 (1998); see also D.H. Lu, D.L. Feng, N.P. Armitage, K.M. Shen, A. Damascelli, C. Kim, F. Ronning, Z.-X. Shen, D.A. Bonn, R. Liang, W.N. Hardy, A.I. Rykov, and S. Tajima, Phys. Rev. Lett. **86**, 4370 (2001).
- ⁵⁴ H.A. Mook and F. Doğan, Nature **401**, 145 (1999), and cond-mat/0103037.
- ⁵⁵ O. Chmaissem, J.D. Jorgensen, S. Short, A. Knizhnik, Y. Eckstein, and H. Shaked, Nature **397**, 45 (1999).
- ⁵⁶ P. Aebi, J. Osterwalder, P. Schwaller, L. Schlapbach, M. Shimoda, T. Mochiku, and K. Kadowaki, Phys. Rev. Lett. **72**, 2757 (1994).
- ⁵⁷ D.J. Singh and W.E. Pickett, J. Supercon. **8**, 583 (1995).
- ⁵⁸ A.A. Kordyuk, S.V. Borisenko, M.S. Golden, S. Legner,

- K.A. Nenkov, M. Knupfer, J. Fink, H. Berger, and L. Forro, *cond-mat/0104294*.
- ⁵⁹ B.O. Wells, Z.X. Shen, A. Matsuura, D.M. King, M.A. Kastner, M. Greven, and R.J. Birgeneau, *Phys. Rev. Lett.* **74**, 964 (1995).
- ⁶⁰ C. Duerr, S. Legner, R. Hayn, S.V. Borisenko, Z. Hu, A. Theresiak, M. Knupfer, M.S. Golden, J. Fink, F. Ronning, Z.-X. Shen, H. Eisaki, S. Uchida, C. Janowitz, R. Mueller, R.L. Johnson, K. Rossnagel, L. Kipp, and G. Reichardt, *Phys. Rev.* **B63**, 14505 (2001).
- ⁶¹ J. Mesot, M.R. Norman, H. Ding, M. Randeria, J.C. Cam-puzano, A. Paramekanti, H.M. Fretwell, A. Kaminski, T. Takeuchi, T. Yokoya, T. Sato, T. Takahashi, T. Mochiku, and K. Kadowaki, *Int. J. Mod. Phys.* **B13**, 3709 (1999).
- ⁶² H. Mook, presented at the Sixth Internat. Conf. on Spectroscopies of Novel Superconductors (SNS01), Chicago, May 13-17 (2001); B. Keimer, *ibid.*
- ⁶³ H. Alloul, *Bull. A.P.S.* **46**, 1070 (2001).
- ⁶⁴ M. Braden, W. Reichardt, E. Elkaim, J.P. Lauriat, S. Shiryayev, and S.N. Barilo, *Phys. Rev.* **B62**, 6708 (2000).
- ⁶⁵ A.I. Solomon and J.L. Birman, *J. Math. Phys.* **28**, 1526 (1987).
- ⁶⁶ R.S. Markiewicz and M.T. Vaughn, *Phys. Rev.* **B57**, 14052 (1998), and *J. Phys. Chem. Solids*, **59**, 1737 (1998).
- ⁶⁷ S.-C. Zhang, *Science* **275**, 1089 (1997).
- ⁶⁸ C. Henley, *Phys. Rev. Lett.* **80**, 3590 (1998).
- ⁶⁹ J. Zaanen and P.B. Littlewood, *Phys. Rev.* **B50**, 7222 (1994).
- ⁷⁰ R.S. Markiewicz and C. Kusko, *cond-mat/0102443*.
- ⁷¹ D.V. Fil, O.I. Tokar, A.L. Shelankov, and W. Weber, *Phys. Rev.* **B45**, 5633 (1992); M.D. Kaplan and G.O. Zimmerman, *J. Phys. Chem. Solids* **59**, 1831 (1998).
- ⁷² G.I. Bersuker and J.B. Goodenough, *Physica C* **274**, 267 (1997).
- ⁷³ A.S. Moskvina, E.N. Kondrashov, and V.I. Cherepanov, *Phys. Sol. St.* **43**, 823 (2001).
- ⁷⁴ M.D. Kaplan and B.G. Vekhter, "Cooperative Phenomena in Jahn-Teller Crystals" (Plenum, N.Y., 1995).
- ⁷⁵ R.S. Markiewicz, to be published, *Phys. Rev. E, cond-mat/0102474*, and presented at the 15th Int. Jahn-Teller Symposium, Boston, 2000, *cond-mat/0102453*.
- ⁷⁶ C.A. Mead, *Rev. Mod. Phys.* **64**, 51 (1992).
- ⁷⁷ M.V. Berry, *Proc. Roy. Soc. London*, **A392**, 45 (1984).
- ⁷⁸ M. Bacci, *Phys. Rev.* **B17**, 4495 (1978).
- ⁷⁹ S. Flach, N.M. Plakida, and V.L. Aksenov, *Int. J. Mod. Phys.* **B4**, 1955 (1990); W.E. Pickett, R.E. Cohen, and H. Krakauer, *Phys. Rev. Lett.* **67**, 228 (1991); A. Bussmann-Holder, A. Migliori, Z. Fisk, J.L. Sarrao, R.G. Leisure, and S.-W. Cheong, *Phys. Rev. Lett.* **67**, 512 (1991).
- ⁸⁰ R.L. Melcher, in "Physical Acoustics", Vol. 12, edited by W.P. Mason and R.N. Thurston (Academic, N.Y., 1976), p. 1.
- ⁸¹ S. Ishihara, T. Egami, and M. Tachiki, *Phys. Rev.* **B55**, 3163 (1997).
- ⁸² C.-Z. Wang, R. Yu, and H. Krakauer, *Phys. Rev.* **B59**, 9278 (1999).
- ⁸³ S. Tang and J.E. Hirsch, *Phys. Rev.* **B37**, 9546 (1988), *ibid.*, **39**, 12327 (1989); S. Mazumdar, *Phys. Rev.* **B39**, 12324 (1989); Q. Yuan, T. Nunner, and T. Kopp, *cond-mat/0101147*.
- ⁸⁴ M. Reedyk and T. Timusk, *Phys. Rev. Lett.* **69**, 2705 (1992).
- ⁸⁵ A.A. Aligia, M. Kulić, V. Zlatić, and K.H. Bennemann, *Sol. St. Commun.* **65**, 501 (1988); B. Normand, H. Kohno, and H. Fukuyama, *Phys. Rev.* **B53**, 856 (1996).
- ⁸⁶ H. Bilz, G. Benedek, and A. Bussmann-Holder, *Phys. Rev.* **B35**, 4840 (1987); A. Bussmann-Holder, A. Simon, and H. Büttner, *Phys. Rev.* **B39**, 207 (1989).
- ⁸⁷ K. Yonemitsu, A.R. Bishop, and J. Lorenzana, *Phys. Rev.* **B47**, 12059 (1993).
- ⁸⁸ C. Falter, M. Klenner, and G.A. Hoffmann, *Phys. Stat. Sol.* **b209**, 235 (1998).
- ⁸⁹ F. Barriquand and G.A. Sawatzky, *Phys. Rev.* **B50**, 16649 (1994).
- ⁹⁰ C. Nayak, *Phys. Rev.* **B62**, 4880 (2000).
- ⁹¹ T.D. Stanescu and P. Phillips, *cond-mat/0102527*.
- ⁹² T. Hsu, J.B. Marston, and I. Affleck, *Phys. Rev.* **B43**, 2866 (1991).
- ⁹³ E. Cappelluti and L. Pietronero, *Phys. Rev.* **B53**, 932 (1996).
- ⁹⁴ H. Bilz, G. Benedek, and A. Bussmann-Holder, *Phys. Rev.* **B35**, 4840 (1987).
- ⁹⁵ A. Bussmann-Holder, A. Simon, and H. Büttner, *Phys. Rev.* **B39**, 207 (1989).
- ⁹⁶ J.E. Hirsch and F. Marsiglio, *Phys. Rev.* **B39**, 11515 (1989), **45**, 4807 (1992).
- ⁹⁷ R.S. Markiewicz and C. Kusko, *cond-mat/0102438*.
- ⁹⁸ R.S. Markiewicz, C. Kusko and V. Kidambi, *Phys. Rev.* **B60**, 627 (1999).
- ⁹⁹ T. Valla, *Bull. A.P.S.* **46**, 289 (2001); Z. Yusov, B.O. Wells, T. Valla, A.V. Fedorov, P.D. Johnson, Q. Li, G.D. Gu, N. Koshizuka, C. Kendziora, S. Jian, and D.G. Hinks, *ibid.*, p. 1039 [figure in N. Smith, *Physics Today* **54**, 1, 33 (2001)].
- ¹⁰⁰ R.S. Markiewicz, *Physica C* **168**, 195 (1990).
- ¹⁰¹ C. Kusko, Z. Zhai, N. Hakim, R.S. Markiewicz, S. Sridhar, D. Colson, Viallet-Guillet, A. Forget, Yu.A. Nefyodov, M.R. Trunin, N.N. Kolesnikov, A. Maignan, A. Daignere, and A. Erb, unpublished.
- ¹⁰² J.M. Tranquada, B.J. Sternlieb, J.D. Axe, Y. Nakamura, and S. Uchida, *Nature* **375**, 561 (1995); J.M. Tranquada, J.D. Axe, N. Ichikawa, A.R. Moodenbaugh, Y. Nakamura, and S. Uchida, *Phys. Rev. Lett.* **78**, 338 (1997).
- ¹⁰³ J. Zaanen and A.M. Oles, *Ann. Physik* **5**, 224 (1996); C. Nayak and F. Wilczek, *Phys. Rev. Lett.* **78**, 2465 (1997); V.J. Emery, S.A. Kivelson, and O. Zachar, *Phys. Rev.* **B56**, 6120 (1997); S.A. Kivelson, E. Fradkin, and V.J. Emery, *Nature* **393**, 550 (1998).
- ¹⁰⁴ V. Kataev, A. Validov, M. Hücker, H. Berg, and B. Büchner, *J. Phys. Cond. Matt* **11**, 6571 (1999).
- ¹⁰⁵ A. Bianconi and M. Missori, *J. Phys. (France)* **I4**, 361 (1994) and in "Phase Separation in Cuprate Superconductors", ed. by E. Sigmund and K.A. Müller (Springer, Berlin, 1994), p. 272.
- ¹⁰⁶ V. Polinger, D. Haskel, and E. Stern, presented at 15th Int. Symp. on the JT Effect, Boston, Aug. 16-22, 2000.
- ¹⁰⁷ S. Wakimoto, G. Shirane, Y. Endoh, K. Hirota, S. Ueki, K. Yamada, R.J. Birgeneau, M.A. Kastner, Y.S. Lee, P.M. Gehring, and S.H. Lee, *Phys. Rev.* **B60**, 769 (1999); S. Wakimoto, R.J. Birgeneau, M.A. Kastner, Y.S. Lee, R.

- Erwin, P.M. Gehring, S.H. Lee, M. Fujita, K. Yamada, Y. Endoh, K. Hirota, and G. Shirane, *Phys. Rev.* **B61**, 3699 (2000).
- ¹⁰⁸ A.P. Kampf, D.J. Scalapino, and S.R. White, cond-mat/0102524.
- ¹⁰⁹ A. Campana, M. Corti, A. Rigamonti, R. Cantelli, and F. Cordero, cond-mat/0005326, to be published, *Euro. Phys. Jnl.*
- ¹¹⁰ A. Zibold, H.L. Liu, S.W. Moore, J.M. Graybeal, and D.B. Tanner, *Phys. Rev.* **B53**, 11734 (1996).
- ¹¹¹ J.L. Tallon, cond-mat/9911422, J.L. Tallon, J.W. Loram, and G.V.M. Williams, cond-mat/9911423, J.L. Tallon, J.W. Loram, G.V.M. Williams, J.R. Cooper, I.R. Fisher, J.D. Johnson, M.P. Staines, and C. Bernhard, *Phys. Stat. Sol.* **b215**, 531 (1999).
- ¹¹² R.S. Markiewicz, *Phys. Rev.* **B62**, 1252 (2000).
- ¹¹³ C. Hess, B. Büchner, M. Hücker, R. Gross, and S.-W. Cheong, *Phys. Rev.* **B59**, 10397 (1999).
- ¹¹⁴ O. Baberski, A. Lang, O. Maldonado, M. Hücker, B. Büchner, and A. Freimuth, *Europhys. Lett.* **44**, 335 (1998).
- ¹¹⁵ K.H. Kim, M. Uehara, C. Hess, P.A. Sharma, and S.-W. Cheong, *Phys. Rev.* **B62**, 11945 (2000).
- ¹¹⁶ N. Ichikawa, S. Uchida, J.M. Tranquada, T. Niemöller, P.M. Gehring, S.-H. Lee, and J.R. Schneider, *Phys. Rev. Lett.* **85**, 1738 (2000).
- ¹¹⁷ P.M. Singer, A.W. Hunt, A.F. Cederström, and T. Imai, *Phys. Rev. Lett.* **82**, 4300 (1999).
- ¹¹⁸ N.L. Saini, H. Oyanagi, and A. Bianconi, *J. Synch. Rad.*, to be published.
- ¹¹⁹ T. Noda, H. Eisaki, and S. Uchida, *Science* **286**, 265 (1999).
- ¹²⁰ Y. Ando, A.N. Lavrov, and K. Segawa, *Phys. Rev. Lett.* **83**, 2813 (1999).
- ¹²¹ Z.A. Xu, N.P. Ong, T. Noda, H. Eisaki, and S. Uchida, *Europhys. Lett.* **50**, 796 (2000).
- ¹²² B. Büchner, M. Breuer, A. Freimuth, and A.P. Kampf, *Phys. Rev. Lett.* **73**, 1841 (1994).
- ¹²³ T. Goto, S. Kazama, K. Miyagawa, and T. Fukase, *J. Phys. Soc. Jpn.*, **63**, 3494 (1994); H. Kimura, K. Hirota, H. Matsushita, K. Yamada, Y. Endoh, S.H. Lee, C.F. Majkrzak, R.W. Erwin, G. Shirane, M. Greven, Y.S. Lee, M.A. Kastner, and R.J. Birgeneau, *Phys. Rev.* **B59**, 6517 (1999); and Y.S. Lee, R.J. Birgeneau, M.A. Kastner, Y. Endoh, S. Wakimoto, K. Yamada, R.W. Erwin, S.H. Lee, and G. Shirane, *Phys. Rev.* **B60**, 3643 (1999).
- ¹²⁴ M.-H. Julien, A. Campana, A. Rigamonti, P. Carretta, F. Borsa, P. Kuhns, A.P. Reyes, W.G. Moulton, M. Horvatic, C. Berthier, A. Vietkin, and A. Revcolevschi, *Phys. Rev.* **B63**, 144508 (2001).
- ¹²⁵ S. Chakravarty, H.-Y. Kee, and C. Nayak, cond-mat/0101204.
- ¹²⁶ P.A. Lee and X.G. Wen, *Phys. Rev. Lett.* **78**, 4111 (1997).
- ¹²⁷ J. Orenstein and A.J. Millis, *Science* **288**, 468 (2000).
- ¹²⁸ R.J. Gooding, *Phys. Rev. Lett.* **66**, 2266 (1991).
- ¹²⁹ J. Mesot, M.R. Norman, H. Ding, M. Randeria, J.C. Campuzano, A. Paramekanti, H.M. Fretwell, A. Kaminski, T. Takeuchi, T. Yokoya, T. Sato, T. Takahashi, T. Mochiku, and K. Kadowaki, *Phys. Rev. Lett.* **83**, 840 (1999).
- ¹³⁰ S. Ono, Y. Ando, T. Murayama, F.F. Balakirev, J.B. Betts, and G.S. Boebinger, *Phys. Rev. Lett.* **85**, 638 (2000); G.S. Boebinger, Y. Ando, A. Passner, T. Kimura, M. Okuya, J. Shimoyama, K. Kishio, K. Tamasaku, N. Ichikawa, and S. Uchida, *Phys. Rev. Lett.* **77**, 5417 (1996).
- ¹³¹ C. Quitmann, P. Almeras, J. Ma, R.J. Kelley, H. Berger, C. Xucyu, G. Margaritondo, and M. Onellion, *Phys. Rev.* **B53**, 6819 (1996).
- ¹³² I. Affleck, Z. Zou, T. Hsu, and P.W. Anderson, *Phys. Rev.* **B38**, 745 (1988).
- ¹³³ Y. Suzumura, Y. Hasegawa, and H. Fukuyama, *J. Phys. Soc. Jpn.* **57**, 401 (1988); N. Nagaosa and P.A. Lee, *Phys. Rev.* **B45**, 966 (1992).
- ¹³⁴ P.A. Lee, N. Nagaosa, T.-K. Ng, and X.-G. Wen, *Phys. Rev.* **B57**, 6003 (1998).
- ¹³⁵ P.W. Anderson, G. Baskaran, Z. Zou, and T. Hsu, *Phys. Rev. Lett.* **58**, 2790 (1987).